International Journal of Engineering Technologies (IJET) is included in:

International Journal of Engineering Technologies (IJET) is harvested by the following service:

Organization	URL	Starting Date
The OpenAIRE2020 Project	https://www.openaire.eu	2015
GOOGLE SCHOLAR	https://scholar.google.com.tr/	2015
WORLDCAT	https://www.worldcat.org/	2015
IDEALONLINE	http://www.idealonline.com.tr/	2018

From the Editor

Dear Colleagues,

On behalf of the editorial board of International Journal of Engineering Technologies (IJET), I would like to share our happiness to publish the 15th and 16th issues of IJET. My special thanks are for members of Editorial Board, Publication Board, Editorial Team, Referees, Authors and other technical staff.

Please find the 15th and 16th issues of International Journal of Engineering Technologies at http://ijet.gelisim.edu.tr or http://dergipark.gov.tr/ijet. We invite you to review the Table of Contents by visiting our web site and review articles and items of interest. IJET will continue to publish high level scientific research papers in the field of Engineering Technologies as an international peer-reviewed scientific and academic journal of Istanbul Gelisim University.

Thanks for your continuing interest in our work,

International Journal of
Engineering Technologies

IJET

Table of Contents

Volume 4, No 3, September 2018

&

Table of Contents

Volume 4, No 4, December 2018

A Combined Approach for Sustainable Supplier Selection: A Case Study for a Manufacturing Firm

Gülçin Bektur

*Industrial Engineering, Iskenderun Technical University, 31200, Iskenderun, Hatay, Turkey

(gulcin.bektur@iste.edu.tr)

Tel: +90 326 613 5600

Abstract- Due to the increasing awareness of environmental and social issues, many researchers have paid much attention to the sustainable supplier selection. This paper addresses sustainable supplier selection problem. Although there are many studies on supplier selection, there is no study that takes into account the advantages of supplying two semi-parts from the same supplier. Supplying semi-parts from the same supplier which has similar production processes and which can transport simultaneously provides advantages to the firms in terms of price, transportation cost and resource consumption. In this study, suppliers were weighted by the AHP (Analytic Hierarchy Process) method. In addition, the contributions of supplying two semi-parts from the same supplier are determined by the AHP method. Mathematical model is used to determine the supplier for each semi-parts. The objective function of the mathematical model is maximizing total weights of the suppliers and contributions of the suppliying two semi- parts from the same supplier. The production capacities of suppliers were taken into account in the study. A case study is provided in a medical devices manufacturer to show the feasibility and effectiveness of the proposed methodology.

1. Introduction

Sustainable supply chain management (SSCM) has been considered as an integration and realization of economic, environmental and social objectives of a company in coordination of critical business processes to improve the company's long- term economic performance (Carter and Easton, 2011). Supplier is the one of the most critical factors for the success of Sustainable Supply Chains (SSC). Due to collaboration with economically, environmentally, and socially strong suppliers could improve the supply chain performance (Song et al., 2017). In the past, only economic criteria are used to evaluate suppliers. After SSCM's starting to attract increasing attention, researchers started to take into account social and environmental criteria while evaluating suppliers' performances. For sustainable supplier selection (SSS) researchers evaluate suppliers according to economic, social and environmental criteria.

A lot of study has been done for SSS problem. Bai and Sarkis (2010), proposed an approach that utilizes grey system and rough set theory. Lu et al. (2010), used fuzzy AHP for evaluating green suppliers' performances. Büyüközkan and Çifçi (2011), developed a novel approach based on fuzzy ANP within multi-person decision-making schema under incomplete preference relations. Amindoust et al. (2012), applied fuzzy logic and a new ranking method on the basis of fuzzy inference system for SSS problem. Govindan et al. (2013), used fuzzy set theory and fuzzy TOPSIS for SSS. Azadnia et al., (2014), proposed an integrated approach of rule-based weighted fuzzy method, fuzzy AHP and multi-objective mathematical model for SSS and order allocation. Jauhar and Pant (2017), proposed an efficient system for SSS by integrating together the traditional multi criteria performance evaluation tool DEA (Decision Envelopment Analysis) with DE (Diffirential Evaluation) algorithm and further with MODE (Multi-Objective Differential Evoluation) to overcome the inherit drawbacks of DEA.

Luthra et al. (2017), proposed a framework to evaluate SSS by using an integrated AHP and VIKOR. Song et al. (2017), proposed a method integrates the merit of pairwise comparison method in determining relative importance, the strength of decision making trial and evaluation laboratory (DEMATEL). Lin et al. (2018), developed a decision model for decision- making in uncertain environments, one specifically tailored for managers in green supply chain management. Vahidi et al. (2018), suggested a hybrid SWOT - QFD (Quality Function Deployment) systematic framework for determining the sustainability criteria. Zhao and Guo (2014), proposed a hybrid fuzzy multi- attribute decision making approach (fuzzy entropy- TOTPSIS) for selecting the best green supplier. Jia et al. (2015), used TOPSIS for ranking potential suppliers among the pool of suppliers. Chung et al. (2016), proposed a green supplier selection and guidance mechanism by integrating the features of ANP and an IPA (importance performance analysis) to achieve sustainable management for green supply chains.

In this study, SSS problem is tackled by an integrated approach. First of all, suppliers are weighted by AHP. If two products are supplied from the same supplier, suppliers can provide cost reduction. Also, if the products are transported simultaneously, supplying semi- parts from the same supplier can also reduce the transportation cost. Taking the scale economy into consideration, supplying two semi- parts from the same supplier can lead to a decrease in resource consumption compared to the situation of supplying from different suppliers. As a result, if two products are supplied from the same supplier, there is a contribution. This contribution was also determined by AHP. Finally, supplier for each products is determined using mathematical model. The objective function of the mathematical model is maximizing the total contribution of supplying two semi- parts from same supplier and total weights of the suppliers. Although there are many studies in the literature about supplier selection, there is no study that takes into consideration the contribution of supplying two semi- parts from the same supplier.

The paper is organized as follows: In Section 2, methodology is presented. In section 3 a case study for a medical devices manufacturer firm is presented. Finally, conclusions are given in Section 4.

2. Methodology

2.1. AHP

AHP is a popular method for tackling multicriteria analysis problems involving qualitative data and has been applied successfully to many actual decision situations (Ayağ, 2007).

The steps of the AHP method are as follows (Saaty, 1981):

Step 1: Define the problem and determine its goal.

Step 2: Structure the hierarchy from the top (the objectives from a decision-maker's viewpoint) through the intermediate levels (criteria on which subdequent levels depend) to the lowest level which usually contains the list of alternatives.

Step 3: Construct a set of pairwise comparison matrices (size n×n) for each of the lower levels with one matrix for each element in the level immediately above by using the relative scale measurement. The pairwise comparisons are done in terms of which element dominates the other.

Step 4: There are n(n-1) judgements required to develop the set of matrices in Step 3. Reciprocals are automatically assigned in each pairwise comparison.

Step 5: Hierarchical synthesis is now used to weight the eigenvectors by the weights of the criteria, and the sum is taken over all weighted eigenvector entries corresponding to those in the next lower level of the hierarchy.

Step 6: Having made all pairwise comparisons, the consistency is determined by using the eigenvalue λ_{max}, to calculate the consistency index, CI, as follows Eq. (1) (Dağdeviren, 2008):

$$CI = \frac{(\lambda_{max} - n)}{n-1} \qquad (1)$$

where n is the matrix size. Judgement consistency can be checked by taking the consistency ratio (CR) of CI with the appropriate value, as follows Eq. (2) [5].

$$CR = \frac{CI}{RI} \qquad (2)$$

The CR is acceptable, if it does not exceed 10%. RI is the average index for randomly generated weights (Saaty, 1989).

2.1.1. Criteria of AHP for calculating weights of the supliers

For determining the criteria, a decision group is formed that consists of six experts (two academicians and four senior level managers from the case company). The inputs of the decision group and a literature analysis are used to select the criteria of SSS for sustainability in supply chain. AHP is used for determining the weights of suppliers. Table 1 summarizes the sustainable supplier selection criteria used by AHP. Price, quality and transportation cost are economical, resource consumption and environmental management system are environmental criteria and occupational health and safety system and information disclosure are social criteria. Implementation of AHP is given on Section 3.

Table 1. Sustainable supplier selection criteria

No	Criteria	Description
1	Price (P)	Capability of supplying the products at reasonable price
2	Quality (Q)	Providing a significant quality level

3	Transportation cost (TC)	The tendency of shipping products at minimum transportation cost
4	Resource consumption (RC)	The use of resources, including energy, power and water, are to be reduces by the practices such as modifying production maintanence and process, conservation, recycling and reusing materials
5	Environmental Mang. System (EMS)	A set of systematic processes and practices that enable a supplier to reduce its environmental impacts, with includes the organizational structure, planning and implementing policy (e.g., ISO 14001 and TQEM) for environmental protection
6	Occup. Health Safety Sys. (OHSS)	It is concerned with the safety, health and welfare of the people engaged at supplier's workplace
7	Inf. Disclosure (ID)	Providing inf. to their customers and stakeholders regarding material used, carbon emissions and toxins released during production etc.

2.1.2. Criteria of AHP for calculating contribution of supplying two semi- parts from the same supplier

If semi-parts are purchased from the same supplier, suppliers can provide price reductions. For this reason, price is a criterion for calculating the contribution of supplying two semi-parts from the same supplier. In particular, the production of semi -parts with similar production processes by the same supplier may result in a reduction in the amount of raw materials and energy used. As a results semi –parts that uses the same machines affect resource consumption criteria positevely. In many firms, machines that are used for production is prepared before the production. This set up time is decreased, if similar products are produced successively. This situation effects the resource consumption positively. As a result, due to the economics of the scale, fixed costs for production of the same or similar types of products in the same supplier are decreasing. If semi-parts supplied from the same suppliers able to transport together can make advantages in terms of transportation cost.

In this study, semi-parts are classified according to their types. Alternatives are the dual combination of product types. The number of alternatives is equal to h(h+1)/2 (h: number of semi–parts types). Supplying the same types of semi- parts from the same supplier does not always provide higher

contribution than the different types of semi-parts. For example, considering transportation cost, small semi-parts that can be transported together with large semi-parts can contribute more than the supplying same types of semi-parts from the same supplier. As a result, the contribution of supplying two semi–parts from the same supplier is calculted by AHP. Implementation of AHP is given on Section 3.

2.2 Mathematical Model

The mathematical model used to identify the appropriate supplier for each semi- parts is given below.

Sets:

J= Set of all parts{1,…,n}

K= Set of all suppliers {1,…,m}

R= Set of part types {1,…,h}

B_r= Set of parts for which the type of the parts are r $\in$ R

Parameters:

p_k: weight of supplier k

q_{ij}: contribution obtained if parts i and j are supplied from the same supplier

c_{kr}: capacity of supplier k for the type r

Decision Variable

x_{jk}: $\begin{cases} 1; & \text{If item } j \text{ is supplied by the supplier } k \\ 0; & \text{otherwise} \end{cases}$

Model:

$$Max\ Z = \sum_j \sum_k p_k\, x_{jk} + \sum_k \sum_{i<n} \sum_{j>i} q_{ij}\, x_{ik} x_{jk} \qquad (1)$$

subject to

$$\sum_{j \in J_r} x_{jk} \leq c_{kr} \qquad \forall\ k,r \qquad (2)$$

$$\sum_k x_{jk} \leq 1 \qquad \forall\ j \qquad (3)$$

$$x_{jk} \in \{0,1\} \qquad (4)$$

The objective function of the model is given in (1) which maximizes total suppliers' weights and contributions of the parts that is supplied from the same supplier. The capacity constraints of suppliers are imposed in (2). Constraint (3) guarantees that each item can be selected for only one supplier. (4) is sign constraint.

3. A Case Study for a Medical Devices Manufacturer Firm

The application was made in a company that manufactures medical devices. The company is experiencing various problems in its procurement process. It decided to work with sustainable suppliers. There have been 3 types of semi-parts

that the suppliers must be determined. 5 alternative suppliers are available. The number of each types of semi-parts and capacity of the suppliers are given in Table 2 and Table 3.

Table 2. Number of semi- parts according to semi- part type

Semi- part type	Number of semi- parts
1	22
2	62
3	85

Table 3. Capacity of the suppliers according to semi-part type

Supplier	Capacity		
	Semi- part type 1	Semi- part type 2	Semi- part type 3
1	5	-	50
2	-	40	10
3	5	45	-
4	12	20	30
5	12	10	5

Phase I: Compute weights of the alternative suppliers using AHP

Structural hierarchy of AHP is given in Figure 1.
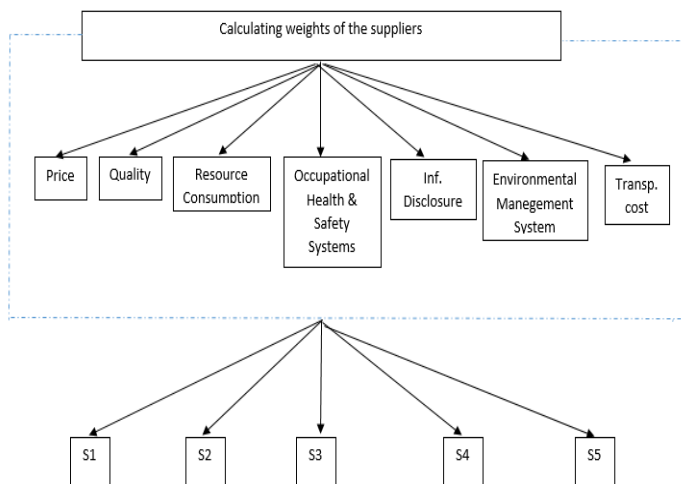
Figure 1. Hierarchy of AHP

Pairwise comparisons of criteria and importance weights of the criteria are given on Table 4. The critical ratio (CR) value is 0.08159.

Table 4: Pairwise comparisons of criteria and importance weights of the criteria

Criteria	Pairwise Comparisons							Importance weights
	P	Q	TC	RC	EMS	OHSS	ID	
P	1	1/2	1	2	3	2	3	0.2027
Q	2	1	1	2	2	2	2	0.2140
TC	1	1	1	1	1	2	1/3	0.1308
RC	1/2	1/2	1	1	2	1	1	0.1154
EMS	1/3	1/2	1	1/2	1	3	1/2	0.1037
OHSS	1/2	1/2	1/2	1	1/3	1	1/2	0.0775
ID	1/3	1/2	3	1	2	2	1	0.1559

The results of comparison of the suppliers according to criteria are given on Table 5. The CR values are smaller than 0.1 for all criteria. The final result of AHP is given on Table 6. By using AHP suppliers are weighted and these weights are used as parameters of the mathemetical model.

Table 5. The results of comparison of the suppliers according to criteria

Criteria	Supplier-1	Supplier-2	Supplier-3	Supplier-4	Supplier-5	CR Value
P	0.2523	0.1062	0.0994	0.2897	0.2524	0.03647
Q	0.2915	0.1052	0.0756	0.1705	0.3572	0.02500
TC	0.1706	0.3578	0.2845	0.1003	0.0868	0.01416
RC	0.0881	0.1854	0.1167	0.2323	0.3775	0.03564
EMS	0.0902	0.3559	0.2709	0.1872	0.0958	0.02141
OHSS	0.0804	0.2853	0.3553	0.1395	0.1395	0.00811
ID	0.2467	0.2688	0.1146	0.1233	0.2466	0.00443

Table 6. Result of AHP

Supplier	Weight
1	0.2000
2	0.2132
3	0.1606
4	0.1845
5	0.2417

As a conclusion, according to the result of AHP the best supplier is 5 with the weight of 0.2417. These weights are used as a parameter fort he mathematical model. By using mathematical model, the semi-parts are supplied from the supplier with the highest weight as much as possible.

Phase II: Compute the contribution of the products that is supplied from the same supplier

Criteria are price, resource consumption and transportation cost. Structural hierarchy of AHP is given in Figure 2. According to Fig 2, 1-1 shows the two semi- parts that the part type is 1. And also, 1-2 shows two semi- parts that the type of one is 1 and another is 2. Other alternatives can be considered in a similar way. Pairwise comparisons of criteria and importance weights of the criteria are given on Table 7. The critical ratio (CR) value is 0.04625.
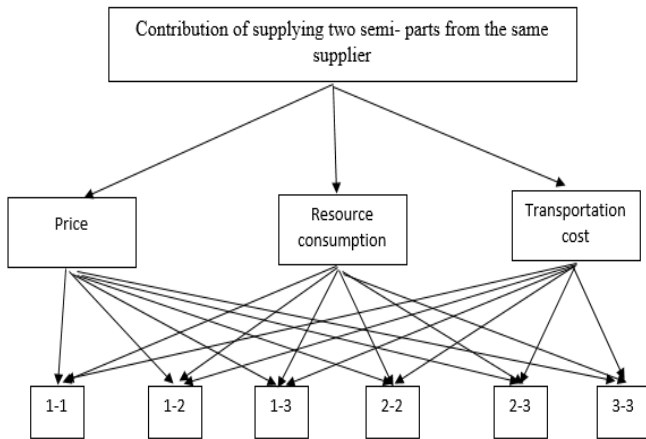
Figure 2. Hierarchy of AHP

Table 7. Pairwise comparisons of criteria and importance weights of the criteria

Criteria	Pairwise Comparisons			Importance weights
	P	TC	RC	
P	1	1	2	0.4111
TC	1	1	1	0.3277
RC	1/2	1	1	0.2612

In terms of price criterion, the alternatives are compared and the following Table 8 is obtained. CR value of comparison of alternatives according to price criterion is 0.03806.

The results of comparison of the suppliers according to criteria are given on Table 9. The CR values are smaller than 0.1 for all criteria. By using AHP contribution of supplying two semi- parts from the same supplier is determined and these contributions are used as parameters of the objective function of the mathemetical model. Mathematical model is used for determining the supplier for each semi –parts. Parameters of the mathematical model are capacities of the suppliers according to product types, weights of the suppliers and contribution of supplying two semi-parts from the same supplier (q_{ij}). q_{ij} values were calculated by AHP.

Table 8. The results of comparison of the suppliers according to criteria

Criteria	1-1	1-2	1-3	2-2	2-3	3-3	CR Value
P	0.2552	0.1162	0.0797	0.2526	0.1236	0.1727	0.03806
RC	0.2675	0.1449	0.0954	0.1914	0.0942	0.2066	0.04017
TC	0.0785	0.1906	0.1719	0.2059	0.1374	0.2157	0.08990

Table 9. Result of AHP

Alternatives	Weights
1-1	0.1992
1-2	0.1481
1-3	0.1141
2-2	0.2214
2-3	0.1205
3-3	0.1957

As a conclusion, according to the AHP results, the highest contribution is satisfied by supplying type 2 semi-parts from the same supplier.

Phase III: Determining the suppliers using mathematical model

The first 22 semi- parts are in type1, semi parts numbered between 23 and 84 are in type 2, semi parts numbered between 85 and 169 are in type 3. q_{ij} values of the semi- parts are given on Figure 3. The values of Figure 3 are obtained by AHP.

Capacities of the suppliers and weights of the suppliers are given on Table 3 and Table 6 respectively.

The model is solved with GAMS/ DICOPT solver. The result of the problem is given on Figure 4.

Figure 3. The parameter of q_{ij}

According to the result, the capacities of suppliers are not exceeded. Each product is supplied from a supplier. And as possible as, semi- parts are supplied from the suppliers that has high values of weights and the semi parts that are provided high value of contribution in case of supplying from the same suppliers are supplied as possible as from the same supplier.

Supplier	J_1 Type 1 products	J_2 Type 2 products	J_3 Type 3 products
1	1 2 3 7 8		85 86 87 88 89 90 91 92 95 97 98 99 103 104 106 107 108 109 111 112 123 125 129 130 131 133 134 135 136 137 138 139 140 141 144 146 148 149 150 152 154 156 157 158 159 161 162 163 165 167
2		27 28 29 30 31 32 33 34 35 36 37 38 39 40 41 42 43 44 45 46 47 48 49 51 53 54 55 56 57 58 59 60 63 64 65 66 71 72 75 83	127 128 132 145 153
3			
4	6 11 14 16 17 18 19 20 21 22	23 24 25 26 50 52 61 62 67 68 69 70 74 76 77 78 80 81 82 84	93 94 96 100 101 102 105 110 113 114 115 116 117 118 119 120 121 122 124 126 142 143 147 151 155 160 164 166 168 169
5	4 5 9 10 12 13 15	73 79	

Figure 4. Result of the mathematical model

As a conclusion, according to the Figure 4, semi- parts 1, 2, 3, 7 and 8 are supplied from supplier 1. And the suppliers of the other semi- parts are given on Figure 4.

4. Conclusions

In this study, the problem of sustainable supplier selection has been examined. A combined approach is proposed for the problem. Alternative sustainable suppliers are weighted by AHP. Contribution of supplying two semi–parts from the same supplier is calculated also AHP. Mathematical model is used for determining the supplier for each semi –parts. The results of AHP are used as parameters of the objective function of the mathematical model. The objective function of the mathematical model is maximizing total weights of the suppliers and contribution of supplying two semi parts from the same supplier. The proposed approach is applied for manufacturer firm. As a result, optimal supplier is dertemined for each semi parts. The proposed approach might be also applied using fuzzy set theory in future research.

References

[1] C. R. Carter, and P. L. Easton, "Sustainable supply chain management: evolution and future directions", International journal of physical distribution and logistic management, vol. 1, pp. 46-62, 2011.

[2] W. Song, Z. Xu, and H. C. Liu, "Developing sustainable supplier selection criteria for solar- air conditioner manufacturer: An integrated approach", Renewable and sustainable energy reviews, pp. 1461-1471, 2017.

[3] C. Bai, and J. Sarkis," Integrating sustainability into supplier selection with grey system and rough set methodologies", International journal of Production Economics, pp. 252-264, 2010.

[4] Y. Lu, H. Wu, and C. Kuo, "Environmental principles applicable to green supplier evaluation by using multi objective decision analysis", International journal of production research, vol 18, pp. 4317- 4331, 2010.

[5] G. Büyüközkan, and G. Çifçi, "A novel fuzzy multi-criteria decision framework for sustainable supplier selection with incomplete information", Computers in Industry, pp. 164-174, 2011.

[6] A. Amindoust, S. Ahmed, A. Saghafinia, and A. Bahreininejad, "Sustainable supplier selection: A ranking model based on fuzzy inference system", Applied soft computing, pp. 1668- 1677, 2012.

[7] K. Govindan, R. Khodaverdi, and A. Jafarian, "A fuzzy multi criteria approach for measuring sustainability performance of a supplier based on triple bottom line approach", Journal of Cleaner Production, pp. 345-354, 2013.

[8] H. Azadnia, M. Saman, and Y. Wong, "Sustainable supplier selection and order lot- sizing: an integrated multi- objective decision- making process", International journal of production research, vol. 2, pp. 383-408, 2014.

[9] K. Jauhar, and M. Pant, "Integrated DEA with DE and MODE for sustainable supplier selection", Journal of Computational Science, pp. 299- 306, 2017.

[10] S. Luthra, K. Govindan, D. Kannan, K. Mangla, and P. Garg, "An integrated framework for sustainable supplier selection and evaluation in supply chains", Journal of Cleaner Production, vol. 3, pp. 1686- 1698, 2017.

[11] P. Lin, C. Hung, T. Lin, and H. Hsieh, "Green suppliers performance evaluation in Belt and Road using fuzzy weighted average with social media information", Sustainability, vol. 1, 2018.

[12] F. Vahidi, A. Torabi, and J. Ramezankhani, " Sustainable supplier selection and order allocation under operational and disruption risks", Journal of Cleaner Production, pp. 1351-1365, 2018.

[13] H. Zhao, and S. Guo, "Selecting green supplier of thermal power equipment by using a hybrid MCDM method for sustainability", Sustainability, vol. 1, pp. 217-235, 2014.

[14] P. Jia, K. Govindan, M. Choi, and S. Ragendran, "Supplier selection problems in fashion business operations with sustainability considerations", Sustainability, vol. 2, pp. 1603-1619, 2015.

[15] C. Chung, C. Chao, and J. Lou, "The establishment of a green supplier selection and guidance mechanism with the ANP and IPA", Sustainability, vol. 3, pp. 259-283, 2016.

[16] Z. Ayağ, "A hybrid approach to machine- tool selection through AHP and simulation", International journal of production research, vol. 9, pp. 2029-2050, 2007.

[17] T. L. Saaty, "The Analytical Hierarchical Process", 1981, McGraw Hill, New York.

[18] M. Dağdeviren, "Decision making in equipment selection: an integrated approach with AHP and Promethee". J. Intell. Manuf., pp. 397-406, 2008.

[19] Saaty, T. L., "Decision making, scaling, and number crunching", Decision Science, pp. 404-409, 1989.

Radial Basis Function Collocation Models for Water Wave Propagation over a Submerged Breakwater

Yavuz Tokmak[‡]

Civil Engineering Department, Faculty of Engineering and Architecture, İstanbul Gelişim University, Avcılar, 34310, İstanbul, Turkey

(ytokmak@gelisim.edu.tr)

[‡] Corresponding Author; Yavuz Tokmak, Cihangir Mah. Şehit Piyade Onbaşı Murat Şengöz Sok. No:8 Avcılar/ İstanbul, Tel: +90 212 422 7000,

Fax: +90 212 422 7401, ytokmak@gelisim.edu.tr

Abstract- In this study, two different numerical models are developed using the radial basis function collocation method (RBFCM) for the waves propagating over variable bathymetry. For the verification and validation of the models, submerged breakwater test, present in the literature, is used. One of the models is based on the Navier-Stokes equations where the fluid is assumed to be viscous, incompressible and is of constant density. Also, it is assumed that the flow is unsteady and the turbulent effects are neglected. And for the other model, it is assumed that the fluid is inviscid, incompressible and is of constant density while the flow is assumed to be unsteady and irrotational. On the surface, fully nonlinear forms of the free surface boundary conditions are implemented using the semi-Lagrangian approach. Multiquadric radial basis functions (MQRBF) are used for the approximation of the unknown parameters. Since each of the models requires the solution of an elliptic boundary value problem, extra collocation centers are defined outside the problem domain in the neighborhood of the boundary centers to define both the boundary condition and the governing equation at a boundary center for better accuracy and stability. It is observed that the results of the both models are in agreement with the laboratory test results.

1. Introduction

First generation water wave propagation models are purely mathematical as the only tool was the mathematical theory in the time they were developed. Therefore the solutions lie within the boundaries of the analytical methods and are limited to the manual efforts as the analytical progress in the topic have ended up with the number of terms included from a perturbation series of the parameters. After the Airy [1] linear wave model, nonlinear Stokes [2] wave models were introduced. These two models are applicable to limited range of water depths especially they fail to give good estimates in shallow water. The most recent effort is due to Fenton [3] in which the fifth order Stokes waves are derived to obtain better results in shallow water. The earliest numerical wave propagation model is developed by Chappelear [4] and Dean [5] where they used the stream function equation as the governing equation and the series

expansion definition of the stream function was required to satisfy the dynamic free surface boundary condition (DFSBC) in the least square sense. Dean [5] showed that stream function solutions can be obtained over the entire depth of water. These models are mainly for horizontal bottoms and the solutions are obtained on a 2D vertical plane.

On the other hand, wave models like cnoidal, solitary, Boussinesq, nonlinear shallow water wave model have come into existence to get better estimates in shallow water. Mei and LeMéhauté [6] and Peregrine [7] were the first generation of Boussinesq wave models. In Madsen and Schäffer [8], Gobbi et al. [9], Madsen et al. [10] efforts have been made to extend the validity of Boussinesq wave models for depeer regions. Except some limited solutions, shallow water wave models are numerical and they are depth

averaged models where the solutions are obtained on a horizontal plane and the bottom can vary.

In parallel to the advancements in computer systems, fully nonlinear irrotational wave models have also been developed where the vertical variation of the wave parameter, namely the velocity potential, is possible. In these models due to Romate [11], Broeze [12], Li and Fleming [13] fully nonlinear forms of the free surface boundary conditions were used and the governing equation is the Laplace equation for the velocity potential where the assumption of irrotationality allowed the utilization of the potential theory.

Apart from the potential theory based models introduced until this point, Navier-Stokes wave models have been developed without restricting the flow to be irrotational and any depth limitations. One of the main difficulties in the Navier-Stokes equations is the pressure field which is not expressed explicitly and along with the momentum equations one other independent equation is the continuity which is expressed in terms of the velocity gradients. Therefore, several techniques have been developed to obtain an independent equation of the pressure. For this purpose, Chorin [14] used the projection method to obtain Poisson equation of the pressure field. Several other approaches to the problem can be found in texts Ferziger and Perić [15], Cebeci et al. [16] and Versteeg and Malalasekera [17].

Another issue in the Navier-Stokes models is the turbulent characteristics of the flow that arise due to boundary irregularities or complex flow regions like the wave breaking zone. For the models estimating the wave energy dissipation due to turbulence one method is that the mean flow and the turbulent fluctuations are split and the Reynolds Averaged Navier-Stokes (RANS) are simulated along with a transport model that estimates the turbulent boundary layer and variation of viscosity in this layer. Another method is the Large Eddy Simulation (LES) where the Navier-Stokes equations are by filtering out small eddies. Also, in Direct Numerical Simulation Models (DNS) sufficiently fine spatial grids are used to catch small eddies and sufficiently small time steps are used to capture every necessary length scales and fluctuations. DNS models require much more computer resources compared to alternative methods.

Most of the models introduced here have been developed using the finite differences, finite elements, and finite volume methods. Since these methods require regular meshes, the water wave propagation problem where at least the free surface boundary deforms in time is simulated using special treatments like interpolation, extrapolation or coordinate transformation into a regular domain. Also, as some of the waves approach to the shore, the free surface becomes multiple valued at the locations where the waves overturn. Most of the free surface tracking methods and also numerical techniques fail to simulate the situations where complex geometries are involved. Based on the work of Hardy [18] in which radial basis functions were used to interpolate geophysical surfaces, Kansa [19,20] used radial basis functions to solve partial differential equations (PDEs) where the unknown parameter is expressed as a series of radial

basis functions (RBFs) using the radial distances between the centers collocated throughout the problem domain. Applying the governing differential equation and the boundary conditions to the approximate expression of the independent variable of the PDE, unsymmetric system of equations were obtained and the results were highly accurate. For the unsteady problems, the interpolation coefficients were assumed to change in time and the integrations were performed to compute the evolution of the coefficients and thereby the flow parameters. RBFs can have global or local support. Earlier RBF models have been developed using the global support functions. Recently, Fornberg et al. [21], Flyer et al. [22] and Fornberg and Flyer [23] used RBF-Finite Differences (RBF-FD) in which the finite difference weights are obtained using RBFs and the resulting system matrices are sparse and computationally efficient compared to models using RBFs of global support.

In this study two numerical models were developed to estimate the water wave propagation over variable bathymetry. The submerged breakwater setup of Luth et al. [24] and Beji and Battjes [25] is used for the validation and verification of the models. One of these models is based on the potential theory and the governing equation is the Laplace equation for the velocity potential where the flow is assumed to be irrotational. The fluid is assumed to be inviscid for this model. And the other model is based on the Navier-Stokes equations where turbulent effects are neglected by assuming rotational effects the due to the irregular boundaries do not have enough time to alter the flow field. The fluid is inviscid for the Navier-Stokes models so that viscosity term remains in the momentum equations. Also, for both of the models the fluid is incompressible, there are no other external effects on the free surface like the wind and the bottom is fixed and impermeable.

2. Problem Definition and Numerical Formulation of the Potential Theory Model

For a domain in two dimensions (2D), velocity field derivable from a potential function $\phi = \phi(x, z, t)$, the continuity equation reduces to the Laplace equation.

$$\nabla^2 \phi = 0 \tag{1}$$

where on the bottom $z = z_b(x)$

$$\frac{\partial \phi}{\partial z} + \frac{\partial \phi}{\partial x} \frac{\partial z_b}{\partial x} = 0 \tag{2}$$

and on the free surface $z = \eta(x)$, the kinematical free surface boundary condition (KFSBC) and semi-Lagrangian form of the DFSBC is valid as shown respectively.

$$\frac{\partial \eta}{\partial t} = \frac{\partial \phi}{\partial z} - \frac{\partial \phi}{\partial x} \frac{\partial \eta}{\partial x} \tag{3}$$

$$\frac{\partial \phi}{\partial t} = -g\eta - \frac{1}{2}|\nabla \phi|^2 + \frac{\partial \phi}{\partial z} \frac{\partial \eta}{\partial t} \tag{4}$$

On the influx boundary, wave parameters are known and in the tests they are obtained from the Stream Function Wave

Theory (SFWT). On the radiation boundary sponge layer is used where after some location $x = x_s$ the sponge layer starts and the DFSBC becomes

$$\frac{\partial \phi}{\partial t} = -g\eta - \frac{1}{2}\left|\nabla\phi\right|^2 + \frac{\partial \phi}{\partial z}\frac{\partial \eta}{\partial t} - c_s(x)\phi \tag{5}$$

with a damping term containing a location dependent coefficient. The sponge coefficient is obtained at a location inside the sponge layer as

$$c_s(x) = \frac{1}{e-1}\left(\frac{e^{|x-x_s|}}{L_s} - 1\right) \tag{6}$$

where L_s is the length of the sponge layer. Also, at the end of the sponge layer Sommerfeld radiation boundary condition is used.

$$\frac{\partial \phi}{\partial t} + c\frac{\partial \phi}{\partial x} = 0 \tag{7}$$

where the coefficient c is the phase speed of the wave if the sponge layer were not used. In the case of sponge layer and estimate of c is used with one of the schemes presented in Miller and Thorpe [26].

For centers located throughout the domain, the velocity potential at a center denoted by located at can be approximately expressed as

$$\phi(\mathbf{x}_i, t) = \sum_{j=1}^{N} \alpha_j(t)\varphi(\left|\mathbf{x}_i - \mathbf{x}_j\right|, \delta) \tag{8}$$

$\left|\mathbf{x}_i - \mathbf{x}_j\right| = r_{ij}$ is the Euclidean distance between two centers, $\alpha_j(t)$ is the interpolation coefficient, is the RBF with a shape parameter δ. The shape parameter is an unknown constant to be determined by trial-and-error during the simulations. If the resulting flow parameters are not known, one method is to calibrate the shape parameter for simpler flows and use it for the complex flows. Another method is to inspect the variation of the results whether they converge to a solution after some trials. Although, some of the RBFs present in the literature do not contain such a shape parameter, multiquadric RBF (MQRBF) of Hardy [18] is used in this study and it contains the shape parameter as given below.

$$\varphi(r_{ij}, \delta) = \sqrt{1 + \delta^2 r_{ij}^2} \tag{9}$$

Obtaining the spatial derivatives of the velocity potential is straightforward as the spatial dependency is introduced by the infinitely differentiable MQRBF. Since the problem is unsteady, integration in time is performed using the sixth order Adams-Bashforth-Moulton predictor and corrector method. Therefore coupling the boundary value problem with the time integrator, the numerical method basically can be expressed as the computation of a boundary value problem followed by the procedure of updating the parameters for the boundary conditions at an instant and performing this at each time step until the final time is reached.

Further modification to the boundary value problem is made by collocating extra centers just outside the domain one for each of the boundary centers. Thereby, the number of independent equations can be used is increased by the number of the boundary centers. This way it is possible to use the governing equation at each of the boundary centers along with the boundary conditions. More detail on the so called PDE collocation on the boundary technique is found in Fedoseyev et al. [27].

3. Problem Definition and Numerical Formulation of the Navier Stokes Model

The Navier-Stokes Equations in 2D vertical domain is composed of the momentum equations in the horizontal (x) and the vertical (z) and the continuity equation as follows.

$$\frac{\partial u}{\partial t} + u\frac{\partial u}{\partial x} + w\frac{\partial u}{\partial z} = -\frac{\partial p}{\partial x} - g\frac{\partial \eta}{\partial x} + \nu\nabla^2 u \tag{10}$$

$$\frac{\partial w}{\partial t} + u\frac{\partial w}{\partial x} + w\frac{\partial w}{\partial z} = -\frac{\partial p}{\partial z} + \nu\nabla^2 w \tag{11}$$

$$\frac{\partial u}{\partial x} + \frac{\partial w}{\partial z} = 0 \tag{12}$$

where u and w are the velocity components along the horizontal and vertical respectively. p is the dynamic pressure per unit density of water and it is obtained from definition of the total pressure per unit density of water p_t that can expressed as the sum of the hydrostatic and dynamic pressure components.

$$p_t = g(\eta - z) + p \tag{13}$$

In order to deal with the pressure term appearing in the Eq. 10- 11, Chorin [14] proposed the projection method where the time rate of change of velocity components are explicitly discretized and provisional values for these components are defined using the momentum equations without the pressure terms. Namely, denoting the n-th time step with superscript n and provisional values with superscript *, the provisional values are obtained as such.

$$\frac{u^* - u^n}{\Delta t} + u^n\frac{\partial u^n}{\partial x} + w^n\frac{\partial u^n}{\partial z} = \nu\nabla^2 u^n \tag{14}$$

$$\frac{w^* - w^n}{\Delta t} + u^n\frac{\partial w^n}{\partial x} + w^n\frac{\partial w^n}{\partial z} = \nu\nabla^2 w^n \tag{15}$$

where Δt is the time increment. Once these provisional values are computed as a correction step velocity components for the new time step $n+1$ are obtained as follows.

$$\frac{u^{n+1} - u^*}{\Delta t} = -\frac{\partial p^{n+1}}{\partial x} - g\frac{\partial \eta^{n+1}}{\partial x} \tag{16}$$

$$\frac{w^{n+1} - w^*}{\Delta t} = -\frac{\partial p^{n+1}}{\partial z} \tag{17}$$

Since this correction step requires the pressure field at the new time step, Eq. (10) is differentiated with respect to x and Eq. (11) is differentiated with respect to z and the results are summed by imposing continuity to get the following Poisson equation for the pressure field at the new time step.

$$\nabla^2 p^{n+1} = \frac{1}{\Delta t}\left(\frac{\partial u^*}{\partial x} + \frac{\partial w^*}{\partial z}\right) - g\frac{\partial^2 \eta}{\partial x^2} \qquad (18)$$

And it is subjected to the ambient pressure on the free surface $z = \eta(x)$, namely

$$p = 0 \qquad (19)$$

On the influx boundary dynamic pressure per unit density values corresponding to the stream function wave is used. Bottom boundary condition is derived using the no-flux boundary condition and the velocity field correction equations (16) and (17). Since the component of the velocity field along the normal of the bottom boundary cancels out, following boundary condition is obtained.

$$-\frac{\partial p^{n+1}}{\partial x} + \frac{\partial p^{n+1}}{\partial z} = \left(-g\frac{\partial \eta^n}{\partial x} + \frac{u^*}{\Delta t}\right)\left(-\frac{\partial z_b}{\partial x}\right) + \frac{w^*}{\Delta t} \qquad (20)$$

Similarly, the radiation boundary condition can be obtained as follows.

$$\frac{\partial p^{n+1}}{\partial x} = -g\frac{\partial \eta^n}{\partial x} + \frac{u^*}{\Delta t} \qquad (21)$$

There is no need to define a sponge type condition for the pressure field since the pressure field is dependent on the velocity filed. Therefore, once the velocity field is damped in the sponge layer by using an artificial damping term, the pressure damps accordingly.

Similar to the potential model, the Navier Stokes model involves the integration of the variables and the solution of a boundary value problem at each time step. In this model velocity components and the free surface are integrated and boundary value problem is solved for the dynamic pressure per unit density. Also, sixth order Adams-Bashforth-Moulton predictor and corrector method is used as an integrator method.

Velocity components on the free surface are also computed using the semi-Lagrangian approach. Namely if the KFSBC is rewritten as

$$\frac{\partial \eta}{\partial t} = w_s - u_s\frac{\partial \eta}{\partial x} \qquad (22)$$

where $u_s = u(x, \eta(x), t)$ and $w_s = w(x, \eta(x), t)$ are the velocity components on the free surface, variation of the velocity components in time with respect to a semi-Lagrangian perspective will become

$$\frac{\partial u_s}{\partial t} = \left.\frac{\partial u}{\partial t}\right|_{z=\eta} + \frac{\partial u}{\partial z}\frac{\partial \eta}{\partial t} \qquad (23)$$

$$\frac{\partial w_s}{\partial t} = \left.\frac{\partial w}{\partial t}\right|_{z=\eta} + \frac{\partial w}{\partial z}\frac{\partial \eta}{\partial t} \qquad (24)$$

In the sponge layer and artificial damping term is added to the momentum equations

$$\frac{\partial u}{\partial t} + u\frac{\partial u}{\partial x} + w\frac{\partial u}{\partial z} = -\frac{\partial p}{\partial x} - g\frac{\partial \eta}{\partial x} + \nu\nabla^2 u - c_s(x)u \qquad (25)$$

$$\frac{\partial w}{\partial t} + u\frac{\partial w}{\partial x} + w\frac{\partial w}{\partial z} = -\frac{\partial p}{\partial z} + \nu\nabla^2 w - c_s(x)w \qquad (26)$$

where definition of the sponge layer coefficient is identical to the Eq. (6).

For N centers collocated throughout the domain where N_b of them are located on the boundaries and N_s of the are located on the free surface, MQRBF discretization of the velocity components, pressure per unit density and the free surface at the i-th center are written as

$$u_i(r_{ij}, t) = \sum_{j=1}^{N} \alpha_j^u(t)\sqrt{1 + \delta^2 r_{ij}^2} \qquad (27)$$

$$w_i(r_{ij}, t) = \sum_{j=1}^{N} \alpha_j^w(t)\sqrt{1 + \delta^2 r_{ij}^2} \qquad (28)$$

$$p_i(r_{ij}, t) = \sum_{j=1}^{N+N_b} \alpha_j^p(t)\sqrt{1 + \delta^2 r_{ij}^2} \qquad (29)$$

$$\eta_i(r_{ij}, t) = \sum_{j=1}^{N_s} \alpha_j^\eta(t)\sqrt{1 + \delta^2 r_{ij}^2} \qquad (30)$$

where r_{ij} is the Euclidean distance between the i-th and the j-th centers. Also, for the velocity components the center set collocated throughout the domain is used, for the pressure field extra centers are collocated for each of the boundary centers outside the domain and for the free surface centers only the centers located on the free surface are used.

4. Test Results and Conclusion

An illustration for the test setup of the submerged break water tests is given in Fig. 1. Water depth is 0.4 m and at 6 m from the input boundary decreases to 0.1 m at the top of the breakwater in 6 m with a slope of 1:20. On the lee side of the breakwater, water depth increases to 0.4 m in 3 m with a slope of 1:10. Wave height of the test wave is H=0.02m and the wave period is T = 2.02s. The right propagating test wave is a weakly nonlinear intermediate water wave.
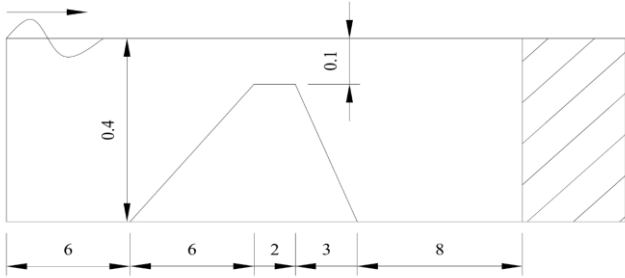
Fig. 1 Test setup for the submerged breakwater simulations. Variable length sponge layer is shaded. (All dimensions are in meters.)

In accordance with the experimental results of Luth et al. [24], simulation results of the Navier Stokes model and nonlinear potential model at the stations x = 5.2, 12.5, 14.5, 17.3 m are plotted in Fig. 2 to Fig. 5.
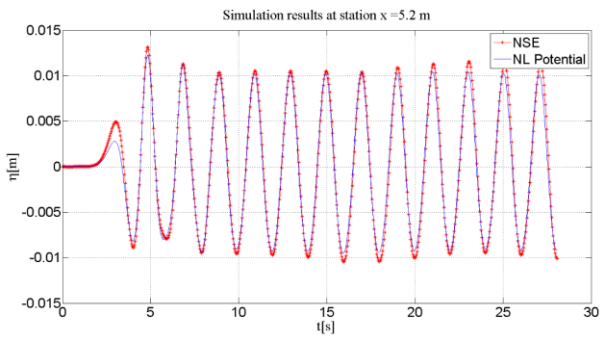
Fig. 2 Comparison of the Navier Stokes and nonlinear potential model results at station x = 5.2 m
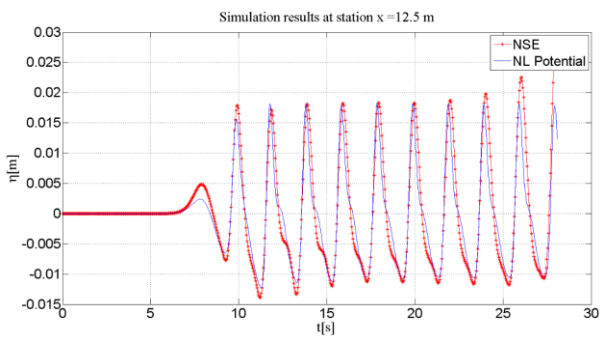
Fig. 3 Comparison of the Navier Stokes and nonlinear potential model results at station x = 12.5 m
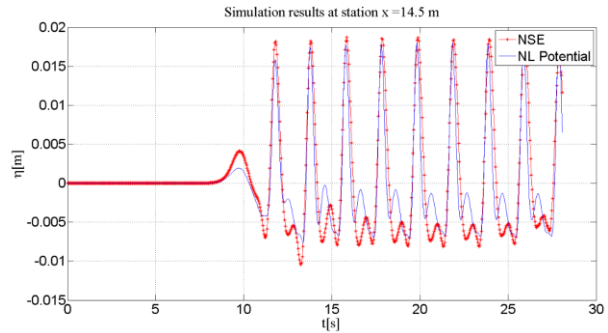
Fig. 4 Comparison of the Navier Stokes and nonlinear potential model results at station x = 14.5 m
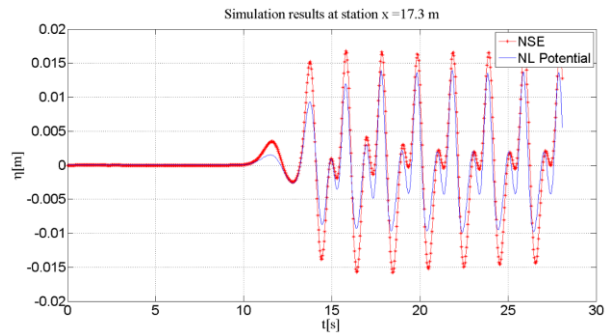
Fig. 5 Comparison of the Navier Stokes and nonlinear potential model results at station x = 17.3 m

In Fig. 6 to Fig. 9 model results are plotted with the experimental results at the stations x = 5.2, 12.5, 14.5, 17.3 m. These results are extracted from the simulation results at a time later than the beginning of the simulations by visual inspection.
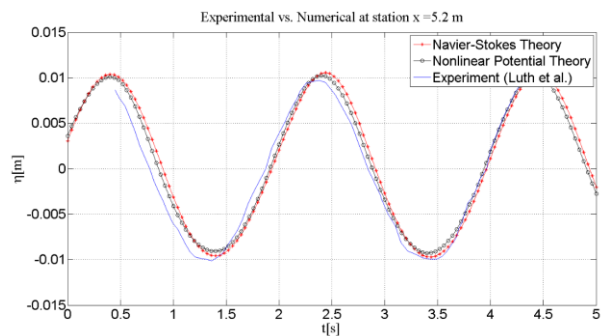
Fig. 6 Comparison of the numerical model results with the experiment results at station x = 5.2 m

140
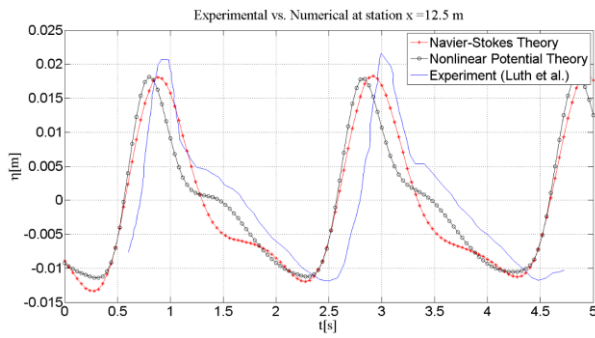
Fig. 7 Comparison of the numerical model results with the experiment results at station x = 12.5 m
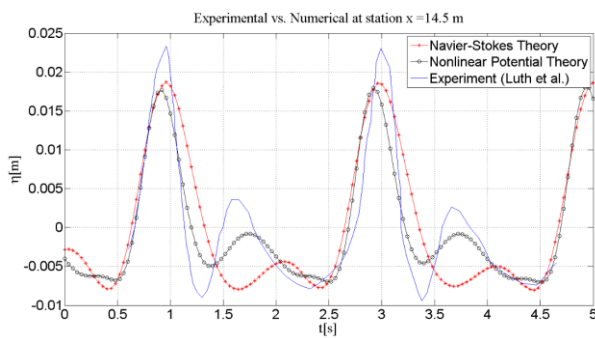
Fig. 8 Comparison of the numerical model results with the experiment results at station x = 14.5 m
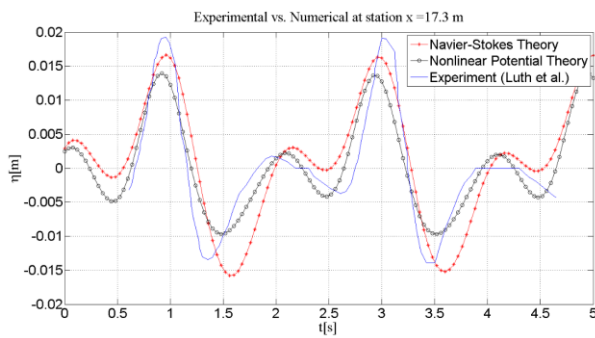
Fig. 9 Comparison of the numerical model results with the experiment results at station x = 17.3 m

The main difference in the results is caused by the reflection from the radiation boundary which is a sponge layer in the numerical models and a sloping beach in the experiment. As apparent from the figures results are in better agreement at the front of the break water, namely at the station x = 5.2 and 12.5 m. On top of the breakwater higher harmonics and higher amplitudes can be observed. The potential theory model results is closer to experiment results compared to those of the Navier Stokes model. On the other hand, at the lee of the breakwater Navier Stokes results are closer to the experiment results compared to those of the potential theory model.

It can be concluded that the RBF collocation method can be used for modeling water wave propagation models. For problems like the free surface flow where the problem domain deforms in time, applying RBFs is easier and higher accuracy can bet obtained compared to methods requiring fixed meshes. There is no need to employ some other method to track for the free surface since the RBF centers moves with the free surface.

Extending the applicability of RBF models are also easier, for example including the transverse direction as the third dimension can simply be implemented by replacing the 2D RBFs with 3D versions in the discrete forms of the parameters.

Coupling this model with a transport model and account for turbulent dissipation from the bottom boundary is also straightforward as long as the viscosities and the thickness of the boundary is determined.

References

[1] G. Airy, Tides and Waves, London:Encyclopedia Metropolitana, 1845, Tom. V, pp.241-396.

[2] G. Stokes, "On the Theory of Oscillatory Waves", Trans. Camb. Philos. Soc., Vol. 8, pp. 441-455, 1847.

[3] J.D. Fenton, "A Fifth-Order Stokes Theory for Steady Waves", ASCE Jour. Waterw., Port, Coastal and Ocean Engr., Vol. 111, pp. 216-234, 1985.

[4] J.E. Chappelear, "Direct numerical calculation of wave properties", J. Geophys. Res., Vol. 66(2), pp. 501–508, 1961.

[5] R. Dean, "Stream Function Representation of Nonlinear Ocean Waves", J. Geophys. Res., Vol. 70, pp. 4561-4571, 1965

[6] C.C. Mei and B. LeMéhauté, "Note on the Equations of Long Waves Over an Uneven Bottom", J. of Geophysical Res., Vol.72, No. 2, pp. 393-400, 1966.

[7] J. Peregrine,"Long waves on a beach", J. Fluid Mech., Vol.27, No. 4, pp. 815-827, 1967.

[8] P.A. Madsen and H.A. Schäffer, "Higher-order Boussinesq-type Equations for Surface Gravity Waves – Derivations and Analysis", Phil. Trans. R. Soc. Lond., Seri A, Vol. 356, pp. 1-59, 1998.

[9] M.F. Gobbi, J.T. Kirby, G. Wei, "A Fully Nonlinear Boussinesq Model for Surface Waves. Part 2 Extension to O(kh)4", J. Fluid Mech., Vol.405, pp. 181-210, 2000.

[10] Madsen, P.A., Bingham, H.B., Liu, H. (2002). A new Boussinesq method for fully nonlinear waves from shallow to deep water. J. Numer. Meth. Fluids, Vol. 462, pp. 1-30, 2002.

[11] J.E. Romate, The numerical simulation of nonlinear gravity waves in three dimensions using a higher order panel method, Ph.D. Thesis, Delft Hydraulics, 1989.

[12] M. Broeze, 1993, Numerical modeling of nonlinear free surface waves with a 3D panel method, Ph. D. Thesis, University of Twente, 1993.

[13] B. Li, and C.A. Fleming, C.A., "A three dimensional multigrid model for fully nonlinear water waves", Coastal Engineering, Vol. 30, pp. 235-258, 1997.

[14] A.J. Chorin, "Numerical Solution of Navier Stokes Equations", Math. Comp., Vol. 22, 745-762, 1968.

[15] J.H. Ferziger and M. Peric, Computational Methods for Fluid Dynamics, Berlin Heidelberg New York: Springer Verlag, 2002.

[16] T. Cebeci, J.P. Shao, F. Kafyeke, E. Laurendeau, E., Computational Fluid Dynamics For Engineers, Long Beach:Horizons Publishing, 2005.

[17] H.K. Versteeg, W. Malalasekera, An Introduction to Computational Fluid Dynamics, 2nd ed., Essex:Pearson Education Limited, 2007.

[18] R.L. Hardy, "Multiquadric equations of topography and other irregular surfaces", Journal of Geophysical Research, Vol. 76(26), pp. 1905-1915, 1971.

[19] E.J. Kansa, E.J. "Multiquadrics - A Scattered Data Approximation Scheme with Applications to Computational Fluid Dynamics-I Surface Approximations and Partial Derivative Estimates", Computers and Mathematics with Applications, Vol. 19, No. 8/9, pp. 127-145, 1990.

[20] E.J. Kansa, "Multiquadrics- A Scattered Data Approximation Scheme with Applications to Computational Fluid Dynamics-II Solutions to Parabolic, Hyperbolic and Elliptic Partial Differential Equations",

Computers and Mathematics with Applications, Vol. 19, No. 8/9, pp. 147-161, 1990.

[21] B. Fornberg, E. Lehto, C. Powell, "Stable Calculation of Gaussian-based RBF-FD stencils", Comput. Math. Appl., Vol. 65(4), pp. 627-637, 2013.

[22] N. Flyer, G.B. Wright, B. Fornberg, B., Radial Basis Function-Generated Finite Differences: A Mesh-Free Method for Computational Geosciences, Handbook of Geomatics: Second Edition, pp. 2635-2669, 2018.

[23] B. Fornberg, and N. Flyer, A Primer on Radial Basis Functions with Applications to the Geosciences, E-book, Society for Industrial and Applied Mathematics, 2015.

[24] H. Luth, G. Klopman, and N. Kitou, 1994, Projects 13G: Kinematics of waves breaking partially on an offshore bar: LVD measurements for waves without a net onshore current., Technical Report H1573, Tech. rep., Delft Hydraulics, 1994.

[25] S. Beji, J.A. Battjes, "Experimental investigation of wave propagation over a bar", Coastal Engineering, Vol.19, pp. 151-162, 1993.

[26] M.J. Miller and A.J. Thorpe, "Radiation conditions for the lateral boundaries of limited-area numerical models", Quarterly J. Royal Meteorological Society, Vol. 107, pp. 615-628, 1981.

[27] A.L. Fedoseyev, M.J. Friedman, E.J. Kansa, 2002, "Improved multiquadric method for elliptic partial differential equations via PDE collocation on the boundary",Comput. Math. Appl., Vol. 43(3–5), pp. 439–455, 2002.

Effects of Cell and Module Configuration on Battery System in Electric Vehicles

Mahmut Kerem Eren*, Eymen Ipek*, Kadir Aras*, Turgay Gucukoglu*, Koray Erhan*‡

*Battery Development Department, AVL Research & Engineering, Sancaktepe, Istanbul, Turkey

(kerem.eren@avl.com, eymen.ipek@avl.com, kadir.aras@avl.com, turgay.gucukoglu@avl.com, koray.erhan@avl.com)

‡Corresponding Author; K Erhan, AVL Research & Engineering, Sancaktepe, Istanbul, Turkey, Tel: +902164987952

Abstract- A battery system is one of the most important powertrain components in Electric Vehicles (xEV). The efficiency of a battery system directly affects the vehicle's range and performance. The configuration of cells and modules also play a key role in battery performance and safety. This study deals with a battery electric passenger vehicle with a battery energy content of 78 kWh. While the vehicle's battery is designed, the criteria to be focused on are evaluated for six different configurations of given cell quantity. The paper focuses on the differences between these configurations regarding the topics which are power losses, control structures, balancing strategies, electrical safety concerns, mechanical aspects, applicability and costs.

Keywords Battery electric vehicle, battery pack, battery module, battery cell

1. Introduction

Full electric and hybrid electric vehicles (HEV) stand out as a rising transportation solution with their energy saving and environmental benefits. In recent years, the number of battery electric vehicles (BEV) and HEVs are increasing day by day. However, there are some challenges to go beyond the limits for the market. One of the main challenge is that BEVs have a short-range capability compared to the conventional vehicles. On the other hand, high battery costs and long charging times are other points which need to be improved. In the near future, the electric vehicle market is expected to face with enhanced conditions which are longer range expectations, lower battery costs and shorter charging duration.

The high voltage (HV) battery is the key powertrain component in BEVs. Due to the lithium-ion batteries high energy and power density values, they are preferred in today's electric vehicles which fits both electrical, mechanical and thermal desired performance criteria [1]. The battery size directly affects the range, performance, weight and price of the vehicle. For this reason, vehicle manufacturers make the cell selection considering some basic boundaries for cell specifications such as kW/kg, kWh/kg, kWh/l, lifetime and kWh/$ values. During the design of a battery, vehicle structure, mechanical and thermal requirements are also essential such that in some cases the prominent structural,

mechanical and thermal requirements even affect the cell selection.

The properties of selected cells are critical in achieving target voltage and capacity values within permissible volume and weight. Once the cell is identified, the configuration of the modules to be created with these cells needs to be determined. In this study, calculations are made to evaluate the effect of different module configurations on the battery system.

Battery capacity and battery weight optimization are important in terms of vehicle efficiency. Increased energy efficiency of up to 10% can be achieved with a suitable capacity for the vehicle and a choice of batteries at the right weight [2].

Another point to note when designing the battery and module is the thermal behavior of the battery. To avoid overheating of the cells, a functional cooling system must be integrated when the module structures are decided [3]. Non-effective cooling accelerates battery aging and may cause failures. Operating the battery in a suitable temperature range is an important parameter that increases the battery life. Lithium-ion batteries are also known to exhibit flammable and explosive behavior at high temperatures [4].

This study intends to summarize the cell and module configuration effects on battery performance for automotive applications. The main aspects presented here are to

investigate the different power losses, control structures, electrical safety concerns, mechanical considerations regarding their applicability and costs between the various cell and module configurations. This paper presents all these approaches along with their respective performances. Finally, a discussion on the aspects advantages and drawbacks is proposed and optimum cases for each condition are presented.

2. System Definition

Development of a battery system requires fundamental requirements and specific parameters which should be considered. Thus, in this chapter, the state of the art situations are mentioned briefly which are evaluated during calculations and analyses such as power demand, module voltage limits with safety boundaries, the control structure of the system, weight limits and joining technologies.

In an average BEV application on the market, approximately quantity of 550-600 PHEV-2 VDA (German Association of the Automotive Industry) sized prismatic cells are fit to the battery volume [5]. Considering the BEVs on the market, approximately 80 kWh battery capacity is determined. These boundaries were considered in the design of this work.

Battery cycle life is directly related to state of charge (SOC) window which defines usable energy value in electric vehicles [6]. Batteries generally are not recommended to be operational above 90% SOC and below 10% SOC due to aging are accelerated on the edges of the SOC values. The SOC window is used to calculate the usable energy out of the installed energy. As an example, when 80% SOC window is used, the installed energy of 78 kWh can be calculated as 62,4 kWh usable energy.

Therefore, the usable energy value is 70 kWh for 90% SOC window and nominal current value is 142 A due to the nominal power value.

2.1. Power Demand

When a market survey is conducted for electrified passenger vehicles, it is observed that the nominal power levels are around 50 kW [5]. Therefore, the nominal power of 50 kW and the maximum power of 150 kW are selected as base power levels for the vehicle which is considered in this study. Moreover, the target voltage level is 350V ±20V due to availability of the components on the market.

2.2. Module Voltage Limit

DC and AC working voltage classes are classified in ISO 6469-3 standard [7]. Low voltage range is called Class A which is given in Table 1.

Maintaining the modules in low voltage class is important in terms of safety and practicality. Otherwise, exceeding the voltage level limit makes it necessary for trained personnel to work on the module. This causes problems throughout manual handling and repairing.

Table 1. Voltage classes [7]

Voltage class	Maximum working voltage	
	DC [V]	AC [V] (rms value)
Class A	$0 < U \leq 60$	$0 < U \leq 30$
Class B	$60 < U \leq 1500$	$30 < U \leq 1000$

2.3. Electrical Safety

During the design process of a battery, electrical safety parameters also affect design criteria. Isolation gaps are defined according to a voltage level in the standards as clearance and creepage distances. When a module or system voltage is increased by changing configurations, clearance and creepage distances also increase. This results in volume expansion.

On the other hand, isolation resistances are also defined in standards with respect to voltage. Therefore, using a high voltage system leads to the necessity of using better insulator materials. Additionally, isolation resistance is depended on the number of modules.

EMC issues result from noise sources which generate electromagnetic disturbance. These electromagnetic disturbances affect victims that are susceptible to electromagnetic disturbance. This relationship creates a design concern which is called Electro Magnetic Compatibility (EMC). When EMC is considered in a battery, both inductive and capacitive coupling must be avoided.

2.4. Control Structure

Battery Control Unit (BCU) and Module Control Unit (MCU) usage is the most common approach of the control structure inside a battery system. Generally, BCU carries out basic battery system functions such as thermal management, switch on/off control, balancing request, power up/down, calculation of state of charge and state of health and etc. while MCU is responsible for measuring and sending cell voltage and temperature data to the BCU. Cell balancing function is also performed via MCU.

The control system topology inside a battery may vary. One of the topologies has multiple modules with integrated single MCU. In another topology, single MCU is utilized per module. When single MCU is used for multiple modules, the cost-related problems may be eliminated. This; however, also brings the complexities of wiring harness and assembly.

Moreover, as the number of series in the module increases, the number of modules that an MCU can manage decreases.

2.5. Cell Balancing

Cell balancing allows each cell to be aged equally. Cell imbalance is caused by specific internal reasons such as manufacturing tolerance, different self-discharge rates and cell impedance. In addition to these, external reasons such as cell configuration, electrical routing and temperature distribution in the system may have also effects on cell balancing.

Cell imbalance is a critical issue to be addressed during the design phase of the system. Otherwise, this may limit the battery system performance and various cell voltages may occur which lead to decreased battery capacity. Therefore, cell balancing plays a critical role in the battery lifetime [8,9].

Balancing method consists of two main categories as 'Passive' and 'Active'. The passive balancing method may be defined as depleting cell(s) charge which has too much charge over a resistor until every cell reaches to the same level of charge. This might be done via switching on a resistor in parallel to the relevant cell on MCU hardware. The active balancing method is simply transferring the energy between cells which are in different energy levels. The active balancing circuitry is based on using a capacitor and/or inductive component to store or transfer the energy.

2.6. Module Mass Limitations

On the automotive market, there is no regulation or standard about maximum weight to lift at work. Instead, there are guidelines or recommendations from different occupational health safety units.

Safe lifting limits are differentiated between men and women. The limit may also be different about how the load is being lifted, how close to the body and how high or low. The recommendation for maximum weight to lift at work is shown in Fig. 1.
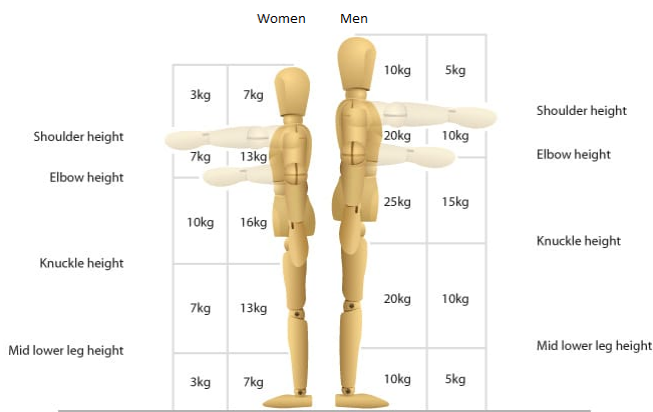
Figure 1. Maximum weight limits to lift at work [10]

2.7. Joining Technology

Different cell assembly methods may be used considering mass production. When assembling cells; resistance welding, ultrasonic welding or laser welding may be used depending on the terminal materials and type of the cells. The material types of the busbar or cables must also be considered when the cells are assembled. For instance, during joining dissimilar materials by using resistance welding (such as nickel and copper) the higher resistive material may be damaged. In another technique, laser welding may be difficult when the thermal conductivity or light absorption is different. On the other hand, in ultrasonic welding, cell terminals may be damaged because of the extreme micro-vibration conditions. Thus, joining technology must be selected regarding project requirements [11].

2.8. Cost Reduction

Cost reduction is an inevitable process for series production. Especially in the automotive market, companies always focus on to decrease costs. Firstly, the increase in voltage level in a module brings some additional cost because of required high-quality isolation materials, training of employees, special equipment for assembly and complexity of the design. Otherwise, smaller modules bring a high quantity of MCUs which causes increase in cost if identical modules are considered. Secondly, module mass also affects the production and maintenance costs. Increasing weight of modules requires special equipment to lift them. If the production is done by robots, this may be more expensive considering the first investment and complexity of production. Finally, joining technology affects the production as well as the maintenance costs. While resistance welding is a low-cost process considering investment and application costs, laser welding and ultrasonic welding have high investment costs.

3. System Evaluation

In chapter 2, the basic concept points which need to be considered during a battery design for automotive market was mentioned shortly. In this chapter, the specific system configurations which are selected to make a comparison with these concept points are evaluated. All the cases are compared regarding their power losses, control structures, weights, applicability and their cost.

3.1. System Configuration

Three different cases are considered in the scope of this work. Moreover, each case is separated into two subcases. As mentioned above in Chapter 2.1, all the cases have the same number of cells, only the module-system configurations and

the connection patterns are different. Case configurations are given in Table 2 and detailed drawings are shown in Fig. 2.

In order to use the flexibility of 12 cells, all module configurations are selected with 12 cells except Case 3.1 as in Table 2. When a module consists of 12 cells, the configuration has the capability to be organized as 12s1p, 6s2p, 4s3p and vice versa.

In Cases 1.1 and 1.2, modules are connected in series, then series modules are connected in parallel as called string connection pattern. Unlike, in Cases 2.1 and 2.2, modules are connected in parallel first, then parallel modules are connected in series which can be seen in Fig. 2.

In Cases 3.1 and 3.2, modules are directly connected as series. To exhibit the effects of huge module configuration and a high number of parallel cells in a module, the module configurations are selected as 12s6p and 2s6p.

Considering the inter-module busbar drawings of Case 2 as shown in Fig. 3, the parallelization of the module connections would lead to complexity and unnecessary busbar amount. It is clear that this situation is not feasible; therefore, Case 2 is excluded from the calculations and analyses.

The module configurations are intended to be lower than 60 V as a voltage level. Consequently, safety limit about voltage level is applied according to ISO 6469-3 standard.

Table 2. Case configurations

Case Numbers	Modules in Series	Modules in Parallel	Cell quantity of Series in Modules	Cell quantity of Parallel in Modules	Number of Cells
1.1	8	6	12	1	576
1.2	24	2	4	3	576
2.1	8	6	12	1	576
2.2	24	2	4	3	576
3.1	8	1	12	6	576
3.2	48	1	2	6	576
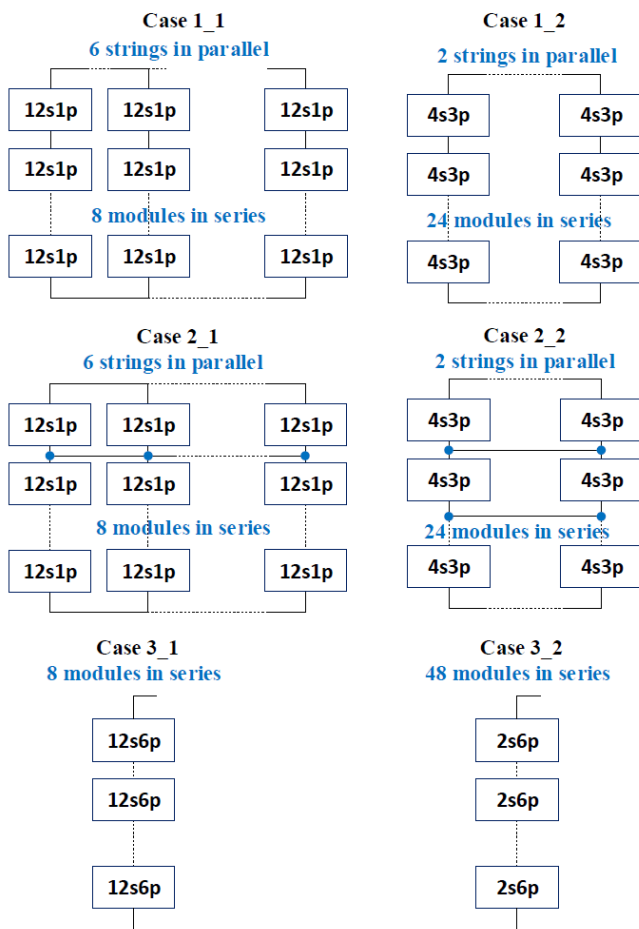
Figure 2. Representative drawings of the cases
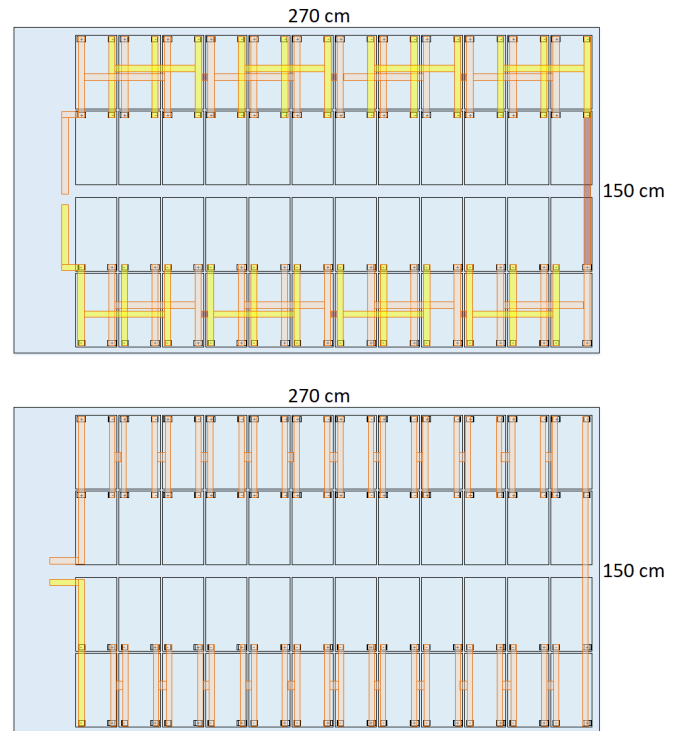
Figure 3. Representative drawing for Case 2

3.2. Power Loss

In order to calculate the power losses of the systems for various configuration of cases, resistances of modules and systems are determined according to equations (1), (2) and (3).

When the calculations are made according to equation (1), (2) and (3) the nominal current value is taken as 142 A since the nominal power value is 50 kW and the nominal voltage value is 352 V.

It is also assumed in this study that laser welding is applied to the prismatic cells with aluminum terminals and that the busbars inside the modules are also aluminum. Due to the high electrical conductivity for the connections between modules, the copper busbars are used with steel bolt nuts. The busbar thickness inside the module is chosen to be 2 mm so that the welding depth value for laser welding is acceptable. However, the thickness of the copper busbars between modules is chosen to be 3 mm to increase the mechanical strength.

Afterward, busbar shapes are classified and values are added to inner cell resistance and laser welding resistance. Thereafter, categorization is determined in terms of busbar shapes and calculated values are added to screw and module resistances. Calculated module-system resistances and power losses regarding the resistances and nominal current value for cases are given in Table 3.

3.3. Control Structure

Selected battery management system (BMS) uses a BCU-MCU structure which is a reference control structure for this study. MCUs are flexible to control a single module or multiple module. The main target is here to create a common MCU-BCU structure to compare the results from the cases.

The MCUs of the selected BMS have 18 measurement points. 2 temperature measurement points for each module are preferred to be used in this work. According to the results of the simulations made, the temperature sensors are placed at the hottest and coldest points of the module. Considering the number of temperature and voltage measurement points, the required number of MCUs are shown in Table 4.

$$R_{Module} = (2.R_{Contact} + R_{Cell\_inner}).\frac{N_{cell\_series}}{N_{cell\_parallels}} + R_{ModuleBusbars}.\left(N_{cell_{series}} - 1\right) + 2.R_{PoleBusbars} \qquad (1)$$

$$R_{Pack} = (2.R_{Contact} + R_{Module}).\frac{N_{module\_series}}{N_{module\_parallels}} + R_{PackBusbars}.\left(N_{Module_{series}} - 1\right) + 2.R_{PoleBusbars} \qquad (2)$$

$$P_{loss} = I^2 R_{pack} \qquad (3)$$

Table 1. Power losses of the cases

Comparison of Cases			
Case Numbers	Module Resistance	System Resistance	Power Loss. @ 142A 25°C %50 SOC
1.1	28.82 mΩ	38.57 mΩ	781.00 W
1.2	3.20 mΩ	39.63 mΩ	802.61 W
3.1	4.80 mΩ	39.24 mΩ	794.59 W
3.2	0.80 mΩ	43.24 mΩ	875.55 W

Referenced cell resistance: 2.4 mΩ

Table 4. Quantity of MCU of cases

Case Numbers	Approach	Voltage measurement points in each module	Temperature measurement points in MCU	No. of MCUs
1.1	1 MCU per module	13	2	48
1.2	1 MCU per 2 modules	5	2	24
3.1	1 MCU per module	13	2	8
3.2	1 MCU per 3 modules	3	2	16

The number of voltage measurement points are determined by using the equation (4).

$$n_{v\_measurement} = n_{series} + 1 \qquad (4)$$

$n_{series}: Cell\ number\ of\ series\ in\ module$

$n_{v\_measurement}: Number\ of\ voltage\ measurement\ point\ on\ module$
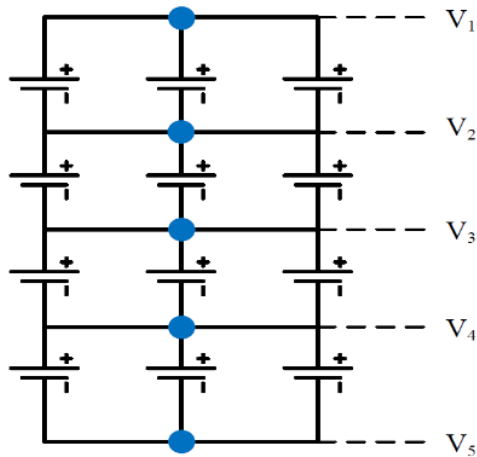
Figure 4. Representation of voltage measurement point on 4s3p module configuration

3.4. Balancing Strategy

In this study, passive balancing method is selected since active balancing requires a more complicated circuit with higher cost, extra software function and algorithm. Using single MCU for multiple modules is another low-cost consideration. In addition to this, the more parallel cell number causes more balancing duration due to a certain balancing current of MCU which is split to parallel branches in the circuit. That's why Cases 1.1 and 2.1 have the shortest duration of balancing which is beneficial in the charging process.

3.5. Electrical Safety

Regarding electrical safety concerns, according to IEC 60664-1 standard [12], clearance distance remains the same for different modules, as it is determined by the structure of the installation. If the number of series exceeds critical voltage levels string fuses may be necessary.

The clearance and creepage distances are valid between conductive HV and low voltage (LV) parts, conductive HV parts and chassis, and between conductive parts of HV+ and HV-. The minimum clearance and creepage distances must be ensured within the module and within the whole battery system considering end of life (EOL). Clearance distance is simply defined in IEC 60664-1 as "minimum air distance between two conductive parts" and the creepage distance is also defined in the same standard as "minimum distance between two conductive parts along the surface of an insulator". According to SAE Application of Insulation Standards to High Voltage Automotive Applications [13], pollution degree can be selected as Pollution Degree 2 or 3 considering the explanation as 'It is proposed that packages with dust protection ratings of IP5KX or better and water

protection ratings of IPX4 or better be considered pollution degree 2'.

Comparative Tracking Index (CTI) is used for measuring the electrical breakdown properties of an insulating material along its surface. The higher CTI value indicates to have the better insulation material and the values are shown in Table 5.

Overvoltage is defined in IEC 60664-1 as "any voltage having a peak value exceeding the corresponding peak value of the maximum steady-state voltage at normal operating conditions". Overvoltage category II is also defined as "Equipment of overvoltage category II is energy-consuming equipment to be supplied from the fixed installation".

Table 5. Material group

Material group I	Material group II	Material group III
CTI $\geq$ 600	600> CTI $\geq$ 400	400> CTI $\geq$ 175

Considering the installation technology, overvoltage category level is proposed as overvoltage category II with rated impulse voltage of 2500 V for equipment. Therefore, the clearance distance is selected as 1.5mm without altitude correction. Considering altitude correction factor for 5000 m, 2.3mm is calculated as clearance distance from the standard IEC 60664-1.

As stated above, the creepage distance is given in the relevant standard to specify the insulation capability of an insulator material. According to module voltage levels, the creepage distances are calculated by interpolating from standard table values which are shown in Table 6.

Clearance and creepage distances are affected by installation technology, the quality of the insulator materials used in the module and packages, the altitude levels, the IP class of the module or packages and the amount of humidity and moisture in the environment. It can be clearly seen that increasing voltage levels increases the module as well as the system dimensions with the effect of clearance and creepage distances while the pollution degree and the material group levels are also affecting on the dimensions.

On the other hand, HV busbar layout in the cases may be evaluated regarding EMC issues. In Case 1.1, there is a long busbar couple which carries both HV and high currents. Therefore, this can cause EMC issues if measurement and signal cables are routed close to HV busbars. However, because there is one MCU per module, measurement cables will be inside of the modules.

In Case 1.2, the middle region of the pack is not occupied. Thus, measurement or signal cables can be routed via this area. As long as, HV busbars are perpendicular to the measurement cables, the inductive coupling is avoided.

Table 6. Creepage distances

Configuration	Voltage Levels (V)	Pollution Degree 2 (mm)			Pollution Degree 3 (mm)		
		MG1	MG2	MG3	MG1	MG2	MG3
2s	8.4	0.4	0.4	0.4	1	1	1
4s	16.8	0.47	0.47	0.47	1.18	1.18	1.18
12s	50.4	0.61	0.87	1.22	1.54	1.74	1.94

In Case 3.1, high current carrying busbars are routed on the side of the pack. Therefore, the middle region is available for LV and signal routing.

In Case 3.2, because single MCU controls more than one module, voltage and temperature measurement wires are routed outside of modules. This case requires the most sensitive wiring harness design considering EMC. To avoid inductive coupling, measurement cables must be perpendicular to the HV busbars. Besides, to prevent capacitive coupling, measurement cables must be placed as far as possible from HV busbars.

3.6. Mechanical Aspects

In addition to the electrical calculations, the cases are also evaluated mechanically. The weight limitation is also tried to be not exceeded for all module configurations. But to have reliable comparison results with the huge module configurations, the module for Case 3.1 consists of a high number of cells which lead to exceeding the weight limitations. This causes to have limitations about manual handling and needs to have operating machines for handling and maintenance. Considering the production plants, series productions are made with robotic technology; therefore, Case 3.1 is also presented.

In order to calculate the gravimetric ratios based on the module, two conceptual modules designed by AVL are investigated. One of the modules examined has 12-cell (6s2p) with 10.75 kg total cell weight and the other one has 24 cells (6s4p) with 21.12 kg total cell weight. The aim here is to observe how the weight ratios change based on the module even though the number of cells is doubled. The cells in approximately same dimensions are used in the examined modules. As a result of the investigations, the ratio of the total cell weight with respect to the module weight may be understood more clearly and the ratios are shown in Table 7. This emphasizes that as the total number of cells in a module are doubled, the percentage of useless weight in a module decreases as 3%. Busbar weights and volumes are calculated according to the busbar cross sections that can carry nominal currents and the results are given in Table 8. Module weights are calculated considering busbar weights, cell weights and housing weights which are represented as useless weight in Table 7 and the result are given in Table 9.

Table 7. Weight ratios

$Useless\ weight = module\ weight$ $-\ total\ cell\ weight$	Useless weight / total cell weight
Referenced Module 1 (6s2p)	%28
Referenced Module 2 (6s4p)	%25

Table 8. Busbar weights and volumes

Case Number	Total module busbar weight	Inter-Module busbar weight	Total module busbar volume	Inter-Module busbar volume
1.1	3.45 kg	12.09 kg	1.27 L	1.35 L
1.2	4.29 kg	2.30 kg	1.58 L	0.26 L
3.1	14.07 kg	2.59 kg	1.57 L	0.35 L
3.2	4.80 kg	12.46 kg	1.77 L	1.39 L

Table 9. Module Weights

Case Numbers	Module weights
1.1	12.36 kg
1.2	12.38 kg
3.1	70.30 kg
3.2	12.39 kg

3.7. Applicability

Safe operation of the battery system requires specific components such as contactors, fuses and current sensors as well as connectors. In certain applications, power electronics components like onboard charger and/or dc-dc converter may also be placed as a part of a battery system. During the design process, a detailed analysis of these components must be done in harmony with each other.

The safety components which are also called as battery distribution unit (BDU) need a certain space inside the battery system. Thus, available space for these elements is crucial during design.

Escalated voltage and power level may cause expansion of the volume for these components. As an analysis bullet point, this is considered to compare different cases.

Applicability of the cases is evaluated in terms of the utilization space for BDU and ease of installation. When the drawings are interpreted, it is clear that Case 3.1 has the most utilization space for BDU. The assembly of Case 3.1 is simpler than the other cases, since, it has the minimum number of busbars. Additionally, cross-over busbar type which is used in

Case 1.1 and Case 3.2 is harder to produce than the straight busbars according to installation. Therefore, those cases are considered more complex than the others.

In Fig. 5, module layout, busbar shapes and busbar geometries are given for Case 1.1. Modules are divided into two parts and pole busbar lines are placed between these parts. Moreover, 6 different busbar types are used; therefore, this makes the production and the assembly phase more complicated.

In Fig. 6, the general system layout is given for Case 1.2. Modules are also divided into two parts and 3 busbar types are considered in this case. Two of them are used as main pole connections while the other one is used for the connections between the modules. This case is more efficient for the assembly stage because of less type of busbar.

Fig. 7 represents the system schematic of Case 3.1. In this configuration, the pack includes larger modules than the other cases; thus, less quantity of busbar is needed for current flow. It decreases the assembly time and increases the production efficiency.

In Fig. 8 which represents Case 3.2, most of the modules are connected using cross busbars. Although 6 busbar types are used, most of them have the same shapes which reduce the assembly time. Additionally, selecting cross busbars provide less complexity and low EMC interference due to its geometrical structure and layout.
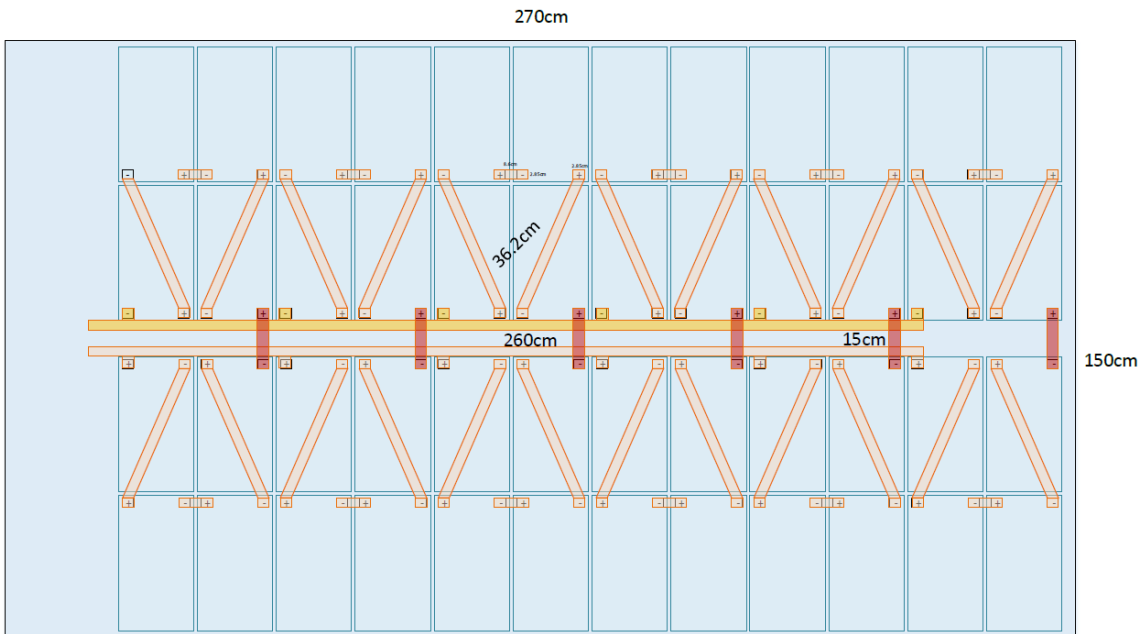
Figure 5. Case 1.1 with detailed representation of the module busbars and dimensions
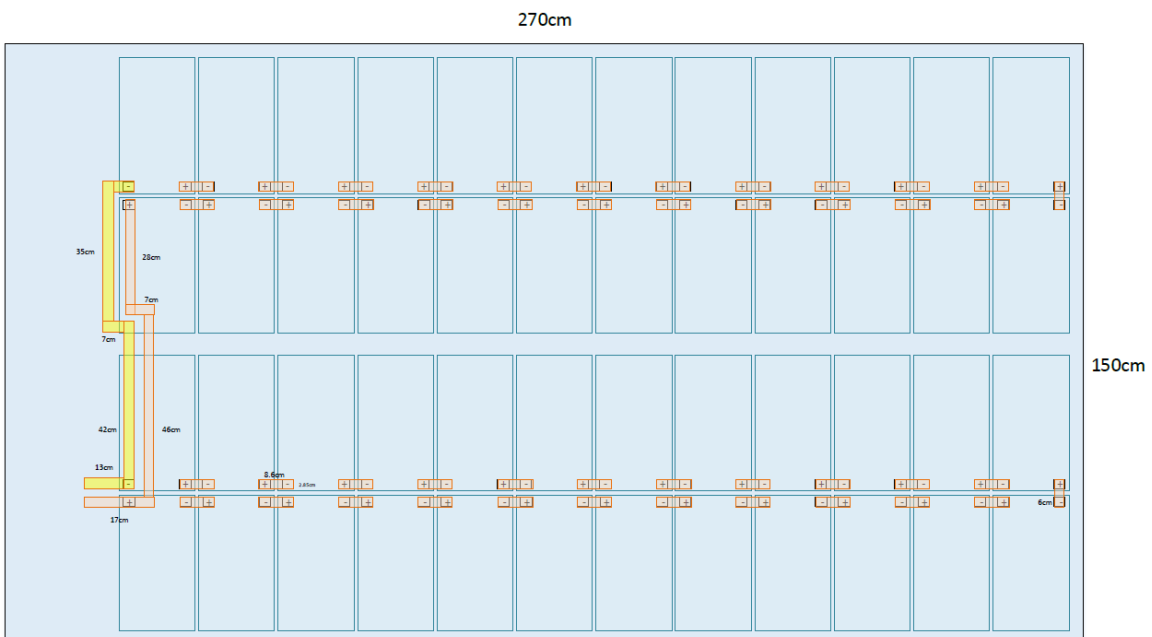
Figure 6. Case 1.2 with detailed representation of the module busbars and dimensions
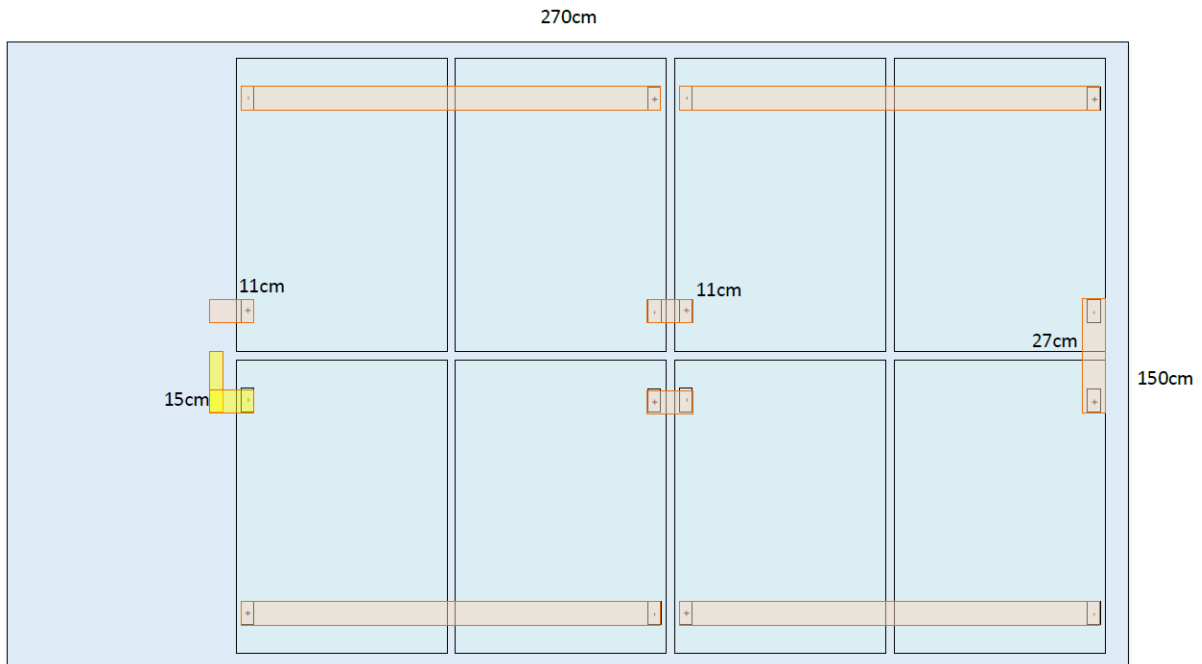
Figure 7. Case 3.1 with detailed representation of the module busbars and dimensions
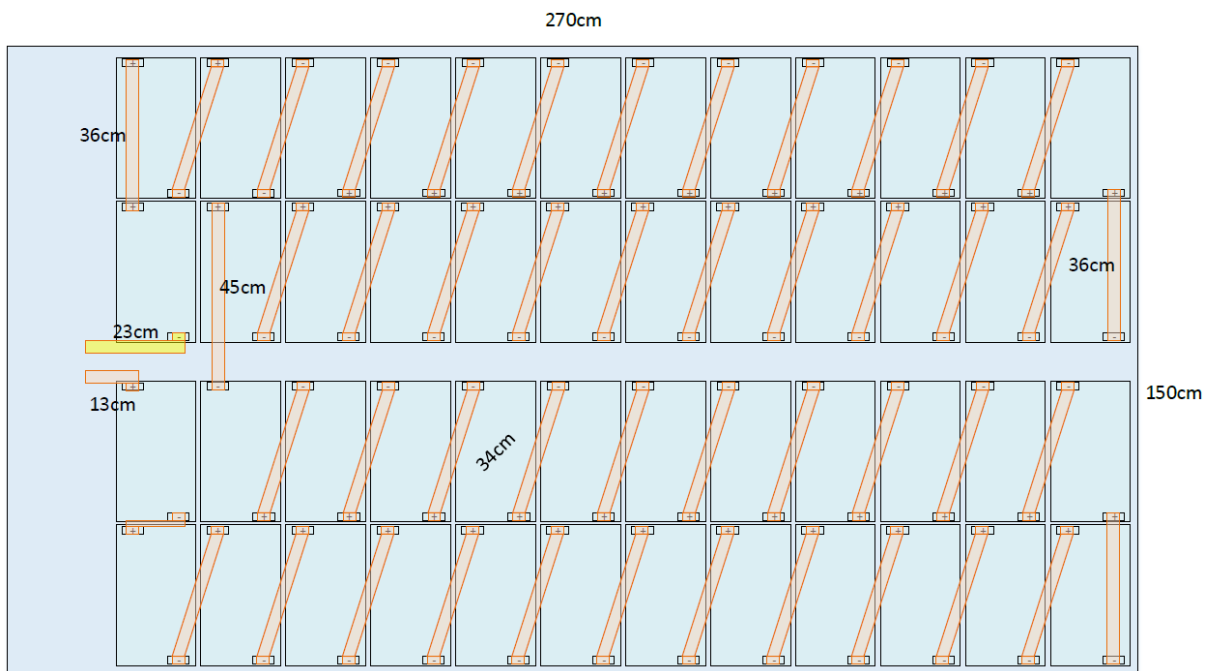
Figure 8. Case 3.2 with detailed representation of the module busbars and dimensions

3.8. Cost

In a battery system, the quantity of used materials and their complexity affect overall cost. In Case 1.1 which has the maximum number of MCUs, the total number of 48 MCUs are integrated while 8 MCUs are placed in Case 3.1 which has the minimum number of MCUs for the same quantity of cell. When this data is considered, Case 3.1 requires the lowest cost in terms of MCU quantity.

Considering cost reduction, the production process has also a crucial impact. When the busbar layout is examined, the assembly of multi-piece structures becomes difficult to handle during the manufacturing process. A high number of busbar pieces require a large number of bolts and nuts with their assembly process. Case 3.1 has an advantage regarding the manufacturing of module to module busbars and assembly process of the modules due to a less number of module connections. When the cases are compared in terms of busbar

weights and volumes, Case 3.2 seems to have the highest cost because it contains the highest quantity of busbar.

4. Conclusion

In the EV market, battery system and module design are very crucial steps in terms of efficiency, ease of production and cost. In the study, 3 basic battery designs with their two sub configurations are investigated and compared.

Case 2.1 and 2.2 are not feasible given the ease of production and efficiency. In addition, since the busbar layout is too complex, it is not suitable for electrical safety and production costs.

In the case of the modules containing the same number of cell, it can be seen that the total power loss is reduced by about 11% if the parallelization is performed between the modules instead of cell strings inside the module. The minimum power loss is obtained in Case 1.1 while the maximum power loss is obtained in Case 3.2 where all modules are connected in series.

On the other hand, the quantity of MCU depends on the series connection of cells in the module. This may also effect on the overall cost of the system. Moreover, using more parallel branch in every series node increases the balancing time.

According to the drawings, the remaining volume for the BDU varies due to different configurations, although cases have the same number of cells. In this study, it can be seen that Case 3.1 has the most free space for BDU. Moreover, large and few modules occupy less space than small and plenty of modules.

The busbar volumes and weights used for inter-module connection vary due to different configurations. The heaviest busbar mass in the system is obtained in Case 3.2 due to the higher number of busbars. The positioning of the modules affects the busbar lengths which is important regarding the weight.

Taking everything into account, when the effect of module and cell configurations on system performance is investigated, it is not possible to talk about an optimum case due to different parameters. Depending on the application, the advantages and disadvantages of each case can be mentioned. The results are presented in terms of feasibility to a real battery system.

References

[1] Kennedy B, Patterson D and Camilleri S, "Use of lithium-ion batteries in electric vehicles", Journal of Power Sources, vol. 90, pp. 156-162, 2000.

[2] Shiau C S N, Samaras C, Hauffe R and Michalek J J, "Impact of battery weight and charging patterns on the economic and environmental benefits of plug-in hybrid vehicles", Energy Policy, vol. 37, pp. 2653-2663, 2009.

[3] Smith K, Wang C Y, "Power and thermal characterization of a lithium-ion battery pack for hybrid-electric vehicles, Journal of Power Sources", vol. 160, pp. 662-673, 2006.

[4] Kiziel R, Sabbah R, Selman J R, Al-Hallaj S, "An alternative cooling system to enhance the safety of Li-ion battery packs", Journal of Power Sources, vol. 194, pp. 1105-1112, 2009.

[5] Zubi G, Lopez R D, Carvalho M, Pasaoglu G, "The lithium-ion battery: State of the art and future perspectives", Renewable and Sustainable Energy Reviews, vol. 89, pp. 292-308, 2018.

[6] Danzer, M.A., Liebau V., Maglia F., "Aging of lithium-ion batteries for electric vehicles", Energy, pp. 359-387, 2015.

[7] ISO Standard 6469-3, Electrically propelled road vehicles -- Safety specifications -- Part 3: Protection of persons against electric shock, International Organization for Standardization, 2011.

[8] Kim J, Shin J, Chun C, Cho B H, "Stable configuration of a li-Ion series battery pack based on a screening process for improved voltage/SOC balancing", IEEE Transactions on Power Electronics, vol. 27, pp. 411-424, 2012.

[9] Kim C H, Kim M Y, Moon G W, "A modularized charge equalizer using a battery monitoring IC for series-connected li-Ion battery strings in electric vehicles", IEEE Transactions on Power Electronics, vol. 28, pp. 3779-3787, 2013.

[10] https://www.highspeedtraining.co.uk/hub/manual-handling-weight-limits/, 17.09.2018.

[11] Brand M J, Schmidt P A, Zaeh M F, Jossen A, "Welding techniques for battery cells and resulting electrical contact resistances", Journal of Energy Storage, vol. 1, pp. 7-14, 2015.

[12] IEC Standard 60664-1, Insulation coordination for equipment within low-voltage systems - Part 1: Principles, requirements and tests, International Electrotechnical Commission, 2007.

[13] SAE Standard 2013-01-1528, Application of Insulation Standards to High Voltage Automotive Applications, Society of Automotive Engineers, 2013.

Low Speed Numerical Aerodynamic Analysis of New Designed 3D Transport Aircraft

Hacı Sogukpinar

Department of Electric and Energy, Vocational School,
University of Adiyaman, Adiyaman 02040, Turkey
(hsogukpinar@adiyaman.edu.tr)

‡Corresponding Author; Hacı Sogukpinar, Department of Electric and Energy,
Vocational School, University of Adiyaman, Adiyaman 02040,
Turkey, Tel: +90 (416) 223 38 00,

Fax: + 90 416 223 21 29, hsogukpinar@adiyaman.edu.tr

Abstract - In this study, a new airfoil was designed by using aerodynamic features of the NACA (National Advisory Committee for Aeronautics) 0012 airfoil and numerical calculation was conducted by using Spalart–Allmaras Turbulence Model. Lift and drag coefficients were calculated and compared with experimental result to correlate numerical calculation accuracy of CFD (Computational Fluid Dynamics) model. Then, according to the new airfoil data, a 3D aircraft fuselage, wings and tail section were modeled by using modified NACA 0012 airfoil. Finally, 3D model aircraft were simulated for cruise flight, climb and descending at the angle of attack +10° and -10° respectively. The simulation results were interpreted in terms of fluid dynamics. Study indicates that during the ascending and descending of the aircraft, very large vortices were formed by the low pressure effect occurring at the rear upper or lower part of the fuselage. Vortices originating from the rear body were caused with the wing tip vortices but the vortex due to the back of the fuselage was found to be very large compared to the wingtip. Furthermore, for each simulation, formation of the wingtip vortices were investigated and presented. Study shows that during ascending the vortex formation was formed in roll up but it was roll down in the phase of descending.

Key words: 3D simulation, Aircraft, vortex, airfoil, Aerodynamic Analysis, lift, drag

1. Introduction

After the first flight of the Wright brothers, new sectors has emerged and research in the whole aviation continued rapidly. As a result of great efforts, dream of the larger airplane and longer distance flights has become real. The high cost of fuel and global warming effects made the need for more efficient airplanes in terms of aerodynamics, and the work has progressed in this direction. Especially at airports, vortices formed during landing and takeoff which affect other flight negatively. For the last 30 years, winglets have been developed and used to reduce wingtip vortex. Aerodynamic flow as a whole for an aircraft has not been investigated but usually only the flow over the wing, the fuselage, the tail and winglet were investigated. But within the framework of an agreement between NASA (National Aeronautics and Space Administration) and Boeing, Boeing 747 passengers' aircraft were analyzed numerically as a whole and presented [1]. The document provides aerodynamic features of lift, drag, pitching moment, rolling and yawing moment, and side force coefficients and also contains information about characteristics of the high lift and propulsion system and landing gear. However, the presented data handles in the form of numeric data and graphs but there is no 2D or 3D direct stream graphics. Flow over generic military airplane was simulated as a whole by using SST turbulence model and compared with experiment [2]. Velocity distribution and eddy viscosity on the surface of the aircraft were given visually and comparatively with the experiment and there was a good agreement between numerical calculation and observation. The main purpose of that work was only to summarize the role of the concepts behind the SST model in current and future CFD simulations of engineering flows. The Boeing 747-200 jumbo jet was numerically investigated and the pressure distribution over the entire surface of the aircraft presented [3]. But the velocity distribution of

the fluid sweeping the surface of the plane was not calculated or given. Therefore, places where swirls are not seen. Another investigation explains the application of optimization techniques for based on control theory for complex aircraft configurations [4] and numerical calculation was conducted for business jet by using Euler equations. This method used Euler equations to reconstruct all configurations of the aircraft by using new multi-block implementation. According to the calculation result, pressure distribution on the entire surface of the plane was presented. With the development of current computer technology CFD's practice revolutionized the aerodynamic design process and it has joined the wind tunnel and flight test as the main means of trade. Boeing Commercial Airplanes use CFD technology, developed by its academia and NASA, and has been used in new plane development. More than 20,000 CFD cases were completed to design a new aircraft in Boeing Company [5]. In other studies, 2D and 3D wing sections were studied extensively [6-12], but it is quite rare to investigate the 3D shape of a plane for aerodynamic analysis. Especially, flow analysis was rarely performed by sending fluid from different angles to the aircraft surface.

In this study, a new airfoil with high lift coefficient at angle of attack zero degree was modeled by using aerodynamic characteristics of NACA 0012 airfoil. The NACA 0012-X airfoil was compared both experimental and theoretical NACA 0012 data to check the simulation correctness of the Computational Fluid Dynamics (CFD) approximation. The airplane fuselage and wings were created using the NACA 0012-X airfoil and numerical calculation conducted by using the Spa-Almrs turbulence model. The streamline velocity distribution on the wing and fuselage were presented and compared according to the simulation result.

2. Spalart–Allmaras Turbulence Model

The Spalart-Allmaras model is a one-equation model that solves a modeled transport equation for the kinematic eddy turbulent viscosity. The model solves only one transport equation for the quantity $\tilde{v}$, it is equivalent to the eddy viscosity away from the walls [13]. This model was designed specifically for aerospace applications that include wall-bounded flows and has been shown to provide good results for boundary layers exposed to negative pressure gradients. This module includes the standard version of the Spalart-Allmaras model without trip term [14, 15]. One model equation for undamped turbulent kinematics is given by equation (1):

$$\frac{\partial \tilde{v}}{\partial t} + \mathbf{u}.\nabla \tilde{v} = c_{b1}\widetilde{S}\tilde{v} - c_{w1}f_w \left(\frac{\tilde{v}}{l_w}\right)^2 + \frac{1}{\sigma}\nabla.\left((v + \tilde{v})\nabla\tilde{v}\right) + \frac{c_{b2}}{\sigma}\nabla\tilde{v}.\nabla\tilde{v} \tag{1}$$

Reynold stresses were evaluated by using Boussinesq eddy viscosity assumption [16] and are expressed by (2):

$$c_{w1} = \frac{c_{b1}}{\kappa_{\tilde{v}}^2} + \frac{1+c_{b2}}{\sigma}, \chi = \frac{\tilde{v}}{v}, f_{w1} = \frac{\chi^3}{\chi^3 + c_{v1}{}^3} \tag{2}$$

The turbulent viscosity was calculated by (3):

$$\mu_T = \rho\tilde{v}f_{v1} \tag{3}$$

To achieve faster decaying behavior of destruction in the outer boundary layer, a function f_w was used [17]. Additional definitions were given in the following equations (4-6) where g acts as a limiter that prevents great values of f_w. Both r and f_w are equal to 1 in the log-layer and decrease in the outer region.

$$f_{w2} = 1 - \frac{\chi}{1+\chi f_{v1}}, f_w = g\left(\frac{1+c_{w3}^6}{g^6 + c_{w3}^6}\right)^{1/6}, g = r + c_{w2}(r^6 - r) \tag{4}$$

$$r = min\left(\frac{\tilde{v}}{\tilde{S}\kappa^2 l^2{}_w}, 10\right), \tilde{S} = max\left(\Omega + C_{Rot}\,min(0, S - \Omega) + \frac{\tilde{v}}{\kappa^2 l^2{}_w}f_{v2}, 0.3\Omega\right) \tag{5}$$

$$S = \sqrt{2S_{ij}S_{ij}} \quad \Omega = \sqrt{2\Omega_{ij}\Omega_{ij}} \tag{6}$$

Where, f_{w1} is damping fuction, κ is von Kármán constant, $\tilde{S}$ is modified vorticity, S is magnitude of vorticity, l_w is distance to the closest wall, $\tilde{v}$, is kinematic viscosity, S_{ij} and Ω_{ij} are mean strain rate and mean rotation rate tensors respectively and represented by:

$$S_{ij} = 0.5(\nabla u + \nabla u^T)\Omega_{ij} = 0.5(\nabla u - \nabla u^T) \tag{7}$$

The default value of model constants are:

$$c_{b1} = 0.1355, c_{b2} = 0.622, c_{v2} = 7.1\sigma = {}^2/_3$$
$$c_{w2} = 0.3, \ c_{w3} = 2, \kappa_v = 0.41, C_{Rot} = 2.0$$

3. CFD Modeling method

NACA 0012 is one of the commonly used airfoil due to its aerodynamic properties. Hundreds of experimental and theoretical investigations have been carried out for this wing section. Wind tunnel experiment of NACA 0012 was conducted in the Langley Low-Turbulence Pressure Tunnel [18] to investigate the low-speed aerodynamic characteristics of the NACA 0012 airfoil, which offers good opportunity to examine CFD simulation technicque. For the numerical calculation Commercial software COMSOL 5.3 was used. To eliminate the effect of the domain size on the numerical simulation, computational domain and boundary conditions extended at least 100c away from airfoil. Computational domain is as shown in Fig. 1. Inlet port was set to velocity inlet and output port was set to output. Low number mesh distribution may produce computation with large error but high number mesh increase computational time. Therefore mesh number in acertain range were used which is compatible with experiment. C type mesh with 86,800 mesh element were created and applied to distribute flow field in the domain and free stream contiditon. High concentrated mesh distribution was applied closed to wall. Mesh distribution around new designed airfoil NACA 0012-X is presented in Fig.2.
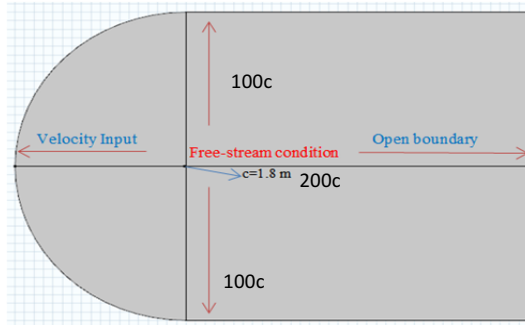
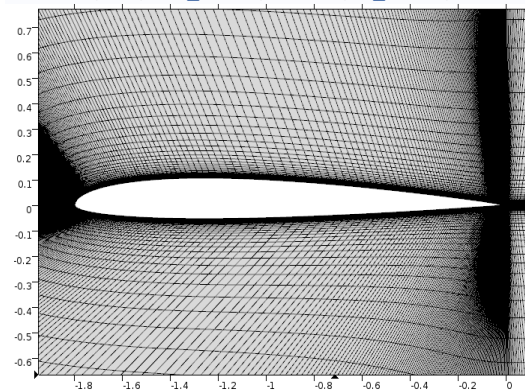Fig. 1: Computational domain and boundary condition.

Fig. 2. Mesh distribution around airfoil NACA 0012-X

The model fuselage was designed according to the NACA 0012-X profile, with a chord length of 1 m. Aircraft wing was designed from NACA 0012-X airfoil with 1.1 m wing span. Wing incidence was set to 3°. The leading edge sweep was depicted as 8.5°. Zero twist and dihedral angle were applied to the model. Basic tail configuration with NACA 0012 airfoil was adopted. For the 3D calculation, separate mesh distribution for the model aircraft and the external environment were applied and free tetrahedral mesh type with extra fine mesh was adopted for both side. 3D body of model with mesh distribution is presenten in Fig. 3.
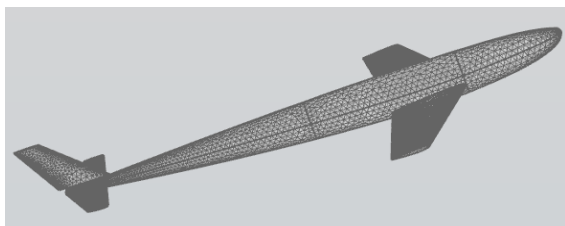

Fig. 3. Mesh distribution around aircraft modeled from NACA 0012-X

4. Results and discussions

Numerical calculation was conducted for NACA 0012 airfoil and lift and drag coefficients were calculated with Spalart–Allmaras turbulence model with the angle of attack from -4° to +18° and presented in Fig. 4, and obtained data were compared with experimental observation [18]. It is observed that theoretical results are in a good agreement with the experimental results. An airfoil with an aerodynamic characteristic close to NACA 0012 but with a high lift coefficient was designed and named as NACA 0012-X. The newly designed airfoil was simulated by using the Spalart-Allmaras Turbulence Model and compared with theoretical and experimental data of NACA 0012 as presented in Fig.4. According to the simulation results, high lift coefficient were obtained in all angle of attack and lift coefficients were calculated at the angle of attack at 0° and 3° as 0.16 and 0.49 respectively.
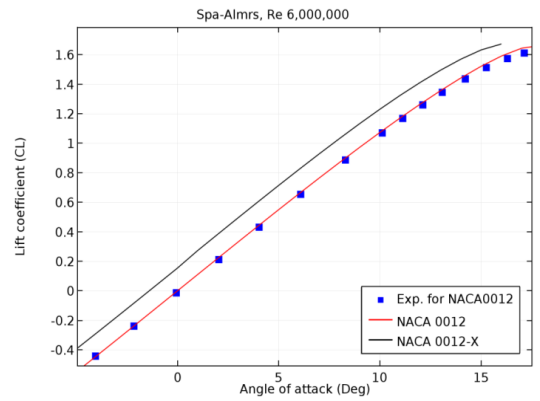
(a)
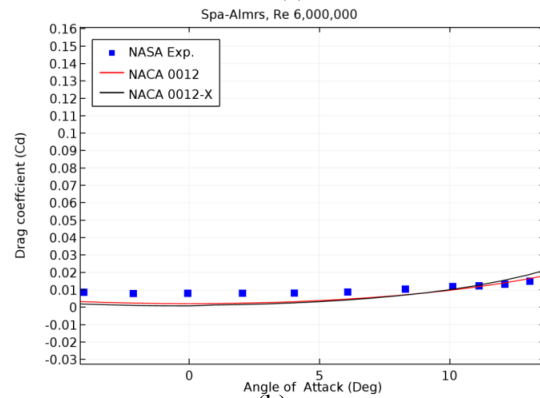
(b)

Fig. 4. Comparison of Lift and Drag coefficient versus angle of attack.

Drag coefficient for newly designed airfoil was calculated lower than both experiment and theoretical data of NACA 0012 airfoil at the angle of attack until 11°. Lift to drag ratio for NACA 0012-X airfoil were calculated and presented comparatively with NACA 0012 airfoil in Fig. 5. Maximum lift to drag ratio was calculated at the angle of attack around 3° therefore streamline velocity is also presented in Fig.5(b).

(a)

(b)

Fig. 6. Streamline velocity fields for NACA 0012-X

Model aircraft fuselage and wings were designed using NACA 0012-X airfoil and tail section was made from NACA 0012. Numerical calculations were performed for model airplane using Spalart-Allmaras Turbulence Model at the angle of attack zero but the maximum lift to drag ratio was achieved at 3° therefore wing incidence was set to 3 °. 3D streamline velocity field of model with top and bottom view is as shown in Fig. 7 and side view is shown in Fig. 8. The graph was plotted by sending fluids over the top and bottom of the wing surface a sequence of layer on the x-y plane. As shown in Fig. 7 and Fig. 8, air flows faster at the top of the plane (reddish color) and slower at the bottom (light color) and laminar flow formed on both sides and fluid continues to sweep the surface of the aircraft front to back properly. Along the fuselage surface, fluid is seen in light color because no slip boundary condition was applied.

(a)

(b)
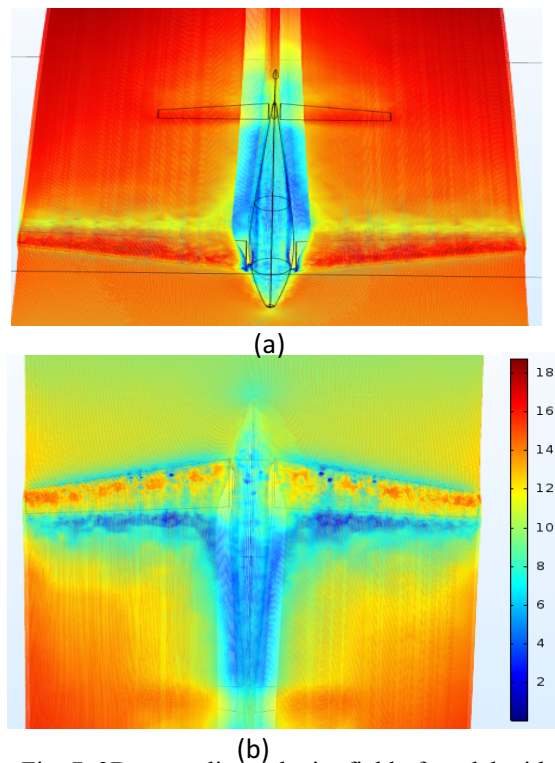
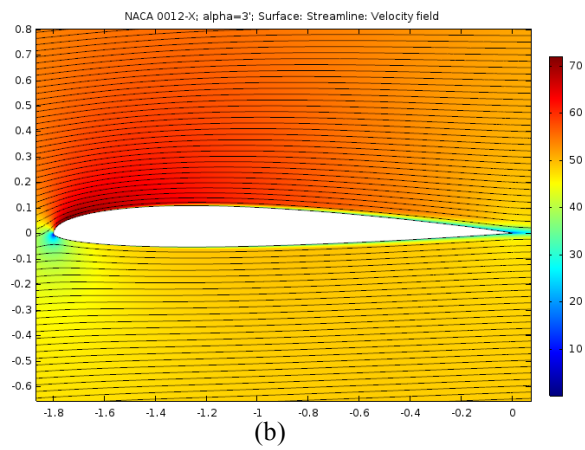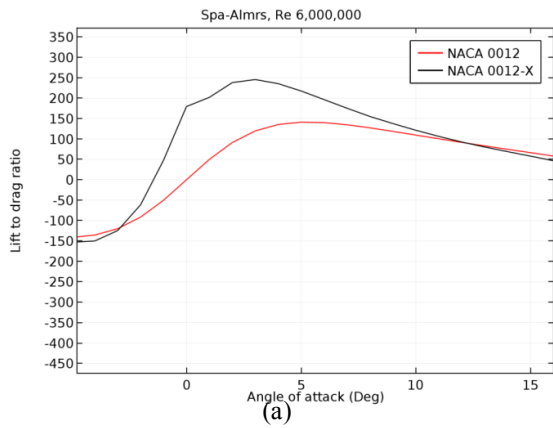Fig. 7. 3D streamline velocity field of model with top (a) and bottom (b) view.

(b)

Fig. 5. Lift to drag ratio (a) and streamline velocity field (b) of NACA0012-X

The stream line velocity field of the NACA 0012-X airfoil is given in Fig.6 at the angle of attack 12° and 14° and almost laminar flows are calculated in both Fig. 6(a) and Fig. 6(b) but the flows separation starts on the upper rear side of airfoil. The low pressure region (reddish) in both images shifted to the front side of the airfoil, which increase the drag as expected to do. Since the low pressure is on leading edge side of airfoil so low pressure pulls wing to that side therefore this automatically increases drag coefficient. The lift coefficients were calculated as 1.41 and 1.57, and the drag coefficients were 0.015 and 0.022, at the angle of attack 3°for the NACA 0012 and NACA 0012-X.
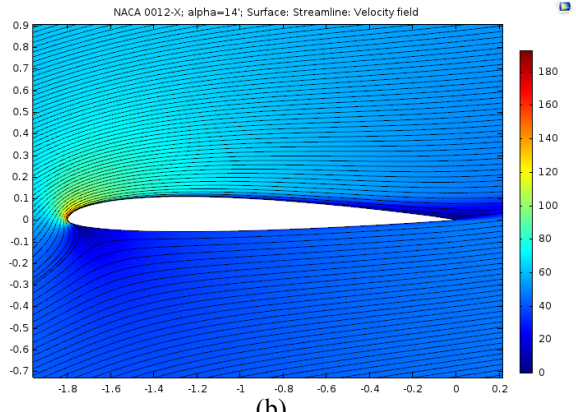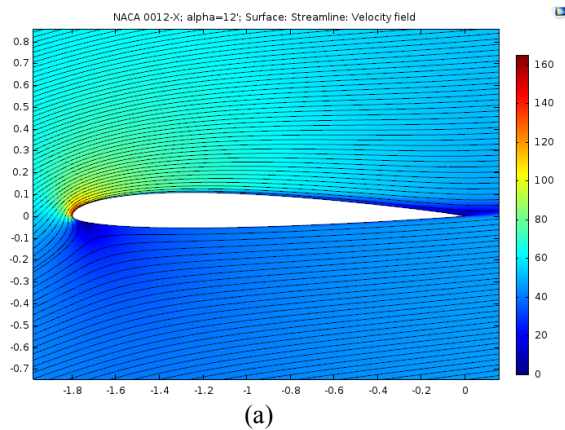

(a)

Fig. 8. 3D streamline velocity field of model with side view.

The fluid was sent as a single layer on x-z plane along the model aircraft and is shown in Fig. 9. It should be emphasized that the fluid only moves over the fuselage and there is no flow on the wing and tail. As we compare the color distribution of the fluid, it is observed that the fluid moves at equal speeds on the top and bottom of the fuselage but fluid moves more slowly behind the plane and along the fuselage surface because of the shadow effect and the no-slip condition respectively.
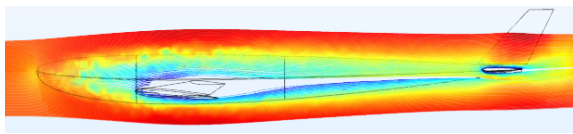
Fig. 9. 3D streamline velocity field over fuselage with side view.

The wingtip vortex was calculated by sending fluid on the x-z plane along the wing surface and is given in Fig. 10. The wingtip vortex formation is enlarged and shown in the same Fig. 10. Due to the pressure difference at the top and bottom of the wing, air flow rolls up into large vortices near the wingtip as seen in Fig. 10. There is no angle of incidence of the plane, but only the wings have three degrees of incidence. Therefore the wingtip vortex is seen to be less in the cruise flight.
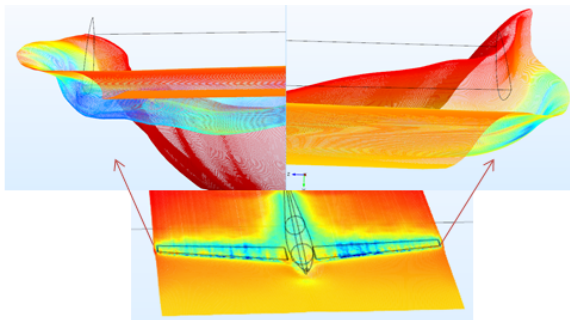
Fig. 10. Wingtip vortex at 3° wing incidence at cruise flight.

Numerical calculation was carried out by giving a 10° angle of attack to the model aircraft and top rear view and top front view are shown in Fig.11 and Fig.12 respectively.
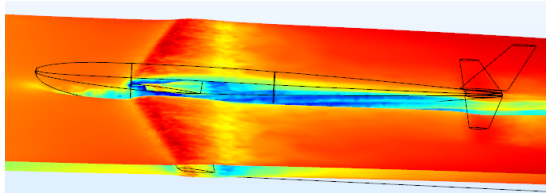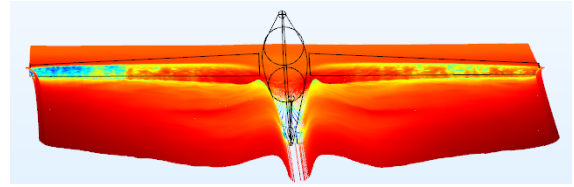

Fig. 11. Top rear view of climbing aircraft at the angle of 10°.

As it is shown in Fig. 11, the formation of the wingtip vortex is clearly visible, but a much larger formation of vortex occurs at the rear of the body. When the plane ascending, it forms a low pressure region at the upper back of the fuselage. And this region leads to the formation of wave peaks from bottom to top. These apices move outward from the body and turn into gigantic vortex waves combining with wingtip vortex at the back of the plane. When the image from the upper front of a flight ascending at the angle of attack 10° is given in Fig. 12, it appears that the vortex formed at the rear of the body is larger than the wingtip vortex.
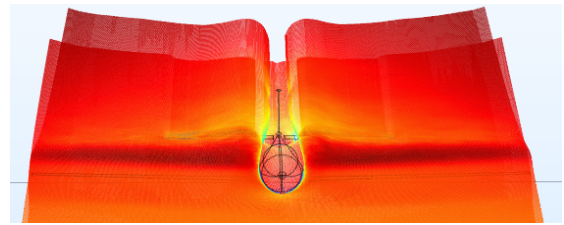
Fig. 12. Top front view of climbing aircraft at the angle of 10°.

The lateral-top and bottom-front views of the plane rising at an angle of 10 ° are given in Fig. 13 and Fig. 14, respectively. When Fig. 13 and Fig.14 are examined, fluid rises to the low pressure region of the back upper part of the body and forms wave peaks. The vortex formed at the upper back of the body is very large compared to the wingtip vortex as shown in Fig.13.
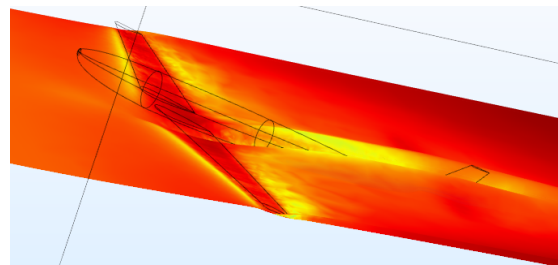
Fig. 13. Lateral top view of climbing aircraft at the angle of 10°.
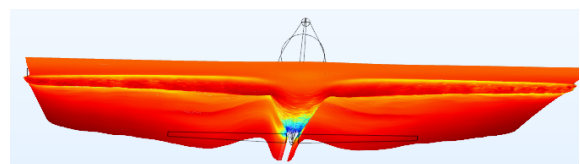
Fig. 14. Sub front view of climbing aircraft at the angle of 10°.

A close-up side view of the fluid passing through the wing surface is shown in Fig. 15. It is seen in Fig. 15 that the fluid passing over the top of the wing continues to travel smoothly, but the fluid passing along the bottom surface curves upwards to form the wingtip vortex.
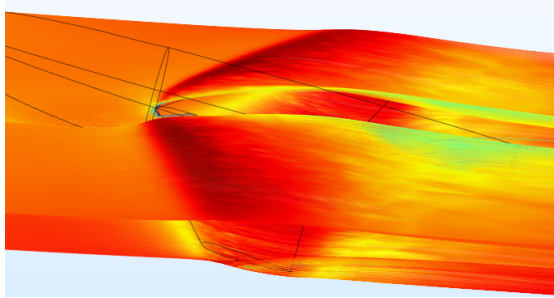
Fig. 15. A close-up side view of the fluid passing through the wing surface.

Wingtip vortex formation (Fig. 16) of the model plane ascending at the angle of attack 10° (the total wing incidence is 13°) is enlarged and for both side is given in Fig. 16. A circular pattern of rotating air is clearly visible at both side of wing.
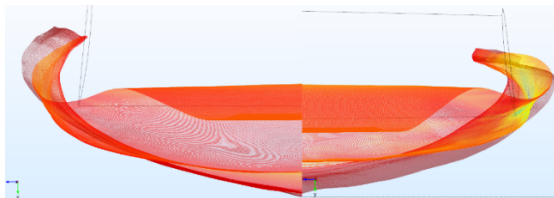
Fig. 16. Wingtip vortex formation of ascending aircraft at the angle of attack 10°.

Descending model aircraft with the angle of attack -10° was numerically analyzed and side view, lower back view, upper-front view, and Sub-front view are presented in Fig. 17, Fig. 18, Fig. 19 and Fig. 20 respectively. When the plane is tilted downward, a low pressure region is formed at the bottom of the tail (back bottom of the fuselage) as seen from the velocity distribution of the fluid (light color), and the shedding effect arises from the body, and ascending to the top of the tail. The fluid flows over the x-y plane, bends in the low pressure region and continues to create large air waves as seen in Fig 17-20. The resulting hill-shaped waves move outward from the wings, and merges with the wingtip vortex and turn into circular vortex flows behind the aircraft. It is seen that the height of the vortex (wave peak) rises from the wings towards the tail. Wingtip vortex formation of descending model plane at the angle of attack -10° (the total wing incidence is -13°) is enlarged and for both side is given in Fig. 21.The direction of the emerging wingtip vortex for the descending mode is opposite to that of the ascending aircraft as shown in Fig.16 and Fig.21.
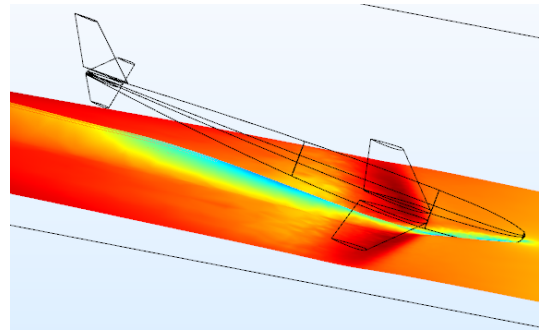
Fig. 17. Side view of descending aircraft at the angle of -10°
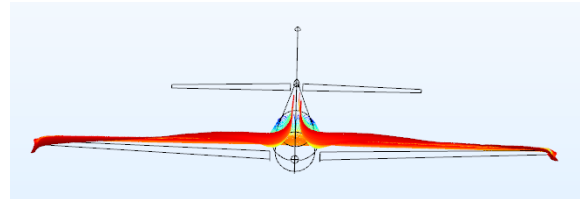
Fig. 18. Lower back side view of descending aircraft at the angle of -10°
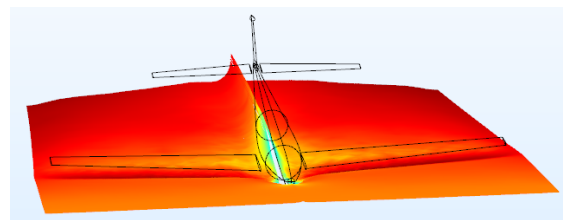
Fig. 19. Upper-front view of descending aircraft at the angle of -10°
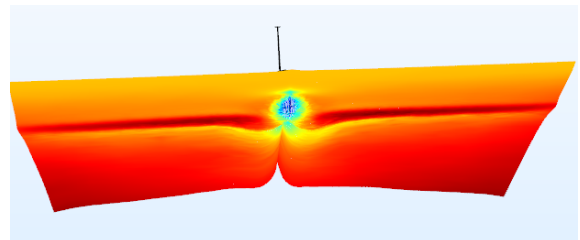
Fig. 20. Sub-front view of descending aircraft at the angle of -10°.

Fig. 21. Wingtip vortex formation of descending aircraft at the angle of attack -10°.

5. Conclusion

Today implementation of CFD has revolutionized the aerodynamic process. In the last 40 years, CFD has been added as a reliable tool for wind tunnel and flight test as a critical tool. Aerodynamic performance of 3D model passenger aircraft was modeled from modified NACA 0012 airfoil and were investigated by using Spalart–Allmaras Turbulence Model. First, 2D simulation data were compared with those obtained from wind tunne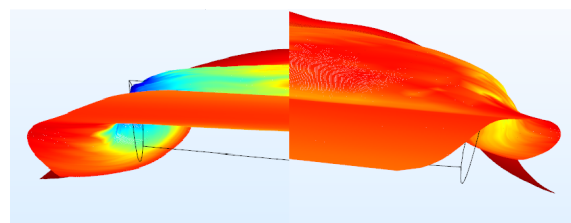l experiment to correlate the simulation correctness of the Computational Fluid Dynamics (CFD) approach. Lift and drag coefficient of NACA 0012 and modified NACA 0012-X were calculated and compared with experiment and comparison shows a good agreement. Then using the newly designed airfoil, the passenger plane's wings and fuselage were created. Aerodynamic properties of the aircraft were investigated by sending air from different angles to the aircraft's wings and its fuselage. According to the result of the simulation, it is seen that during ascending or descending, large wave dips are seen on the rear side of the fuselage. According to the flow analysis, these ripples are due to the difference in pressure at the top and bottom of the tail. Wingtip vortex was also numerically analyzed and it is observed that during the ascending, wing vortex is curved upwards, and during descending it is curved down from bottom. In the flow analysis, the vortex formed at the back of the fuselage is seen to be larger and stronger compared to wingtip vortex. The vortex formed at the wingtip and at rear back of the body combine to form stronger circular vortices.

Acknowledgment

Funding

References

[1] C. R. Hanke and R. N. Donald, "The Simulation Of A Jumbo Jet Transport Aircraft",Vol.1, D6 - 30643, 1970.

[2] F.R. Menter, "Review of the shear-stress transport turbulence model experience from an industrial perspective", International Journal of Computational Fluid Dynamics, Vol. 23:4, pp. 305-316, 2009.

[3] A. Jameson, T. J. Baker and N. P. Weatherill, "Calculation of Inviscid Transonic Flow over a Complete Aircraft", AIAA 24th Aerospace Sciences Meeting, 86-0103. 1986.

[4] J. Reuther, A. Jameson, J. Farmer, L. Martinelli, D. Saunders, C.A. Moffett Field, "Aerodynamic shape optimization of complex aircraft configurations via an adjoint formulation", AIAA Paper, pp. 94, 1996.

[5] T. Forrester Johnson, N. Edward Tinoco, N. Jong Yu. "Thirty years of development and application of CFD at Boeing Commercial Airplanes, Seattle", Computers & Fluids, Vol. 34, pp. 1115–1151, 2005.

[6] H. Sogukpinar, and I. Bozkurt. "Calculation of Optimum Angle of Attack to Determine Maximum Lift to Drag Ratio of NACA 632-215 Airfoil." Journal of Multidisciplinary Engineering Science and Technology, Volume 2, pp.1103-1108, 2015.

[7] H. Sogukpinar, and I. Bozkurt, "Calculation of Aerodynamic Performance Characteristics of Airplane Wing and Comparing with the Experimental Measurement." International Journal of Engineering Technologies Volume 1.2, pp. 83-87, 2015.

[8] H. Sogukpinar, "Numerical calculation of wind tip vortex formation for different wingtip devices", INCAS Bulletin, Volume 10(3), pp. 167-176, 2018.

[9] H. Sogukpinar, "Numerical Simulation of 4-Digit Inclined NACA 00xx Airfoils To Find Optimum Angle of Attack for Airplane Wing" Uludag University Journal of The Faculty of Engineering, Volume 22.1, pp. 169-178, 2017.

[10] H. Sogukpinar, "The effects of NACA 0012 airfoil modification on aerodynamic performance improvement and obtaining high lift coefficient and post-stall airfoil.", AIP Conference Proceedings, Vol. 1935. No. 1. AIP Publishing, 2018.

[11] H. Sogukpinar, "Estimation of supersonic fighter jet airfoil data and low speed aerodynamic analysis of airfoil section at the Mach number 0.15." AIP Conference Proceedings. Vol. 1935. No. 1. AIP Publishing, 2018.

[12] H. Sogukpinar, and Ismail Bozkurt. "Implementation of different turbulence model to find proper model to estimate aerodynamic properties of airfoils." AIP Conference Proceedings, Vol. 1935. No. 1, AIP Publishing, 2018.

[13] B. Aupoix, P.R. Spalart, "Extensions of the Spalart–Allmaras turbulence model to account for wall roughness", International Journal of Heat and Fluid Flow, Volume 24, pp. 454–462, 2003.

[14] D.C. Wilcox, Turbulence Modeling for CFD, 2nd ed., DCW Industries, 1998.

[15] The Spalart-Allmaras Turbulence Model, NASA Langley Research Center. https://turbmodels.larc.nasa.gov

[16] S.R. Allmaras, T.J. Forrester, and P.R. Spalart. "Modifications and Clarifications for the Implementation of the Spalart-Allmaras Turbulence Model." Seventh International Conference on Computational Fluid Dynamics (ICCFD7), 2012.

[17] S. Deck, P. Duveau, P. d'Espiney, & P. Guillen, "Development and application of Spalart–Allmaras one equation turbulence model to three-dimensional supersonic complex configurations", Aerospace Science and Technology, Volume 6(3), pp. 171-183, 2002.

[18] C.L. Ladson, "Effects of Independent Variation of Mach and Reynolds Numbers on the Low-Speed Aerodynamic Characteristics of the NACA 0012 Airfoil Section, NASA TM 4074, 1988.

INTERNATIONAL JOURNAL OF ENGINEERING TECHNOLOGIES-IJET

Guide for Authors

The **International Journal of Engineering Technologies (IJET)** seeks to promote and disseminate knowledge of the various topics of engineering technologies. The journal aims to present to the international community important results of work in the fields of engineering such as imagining, researching, planning, creating, testing, improving, implementing, using and asking. The journal also aims to help researchers, scientists, manufacturers, institutions, world agencies, societies, etc. to keep up with new developments in theory and applications and to provide alternative engineering solutions to current.

The *International Journal of Engineering Technologies* is a quarterly published journal and operates an online submission and peer review system allowing authors to submit articles online and track their progress via its web interface. The journal aims for a publication speed of **60 days** from submission until final publication.

The coverage of IJET includes the following engineering areas, but not limited to:

All filed of engineering such as;

Chemical engineering

- Biomolecular engineering
- Materials engineering
- Molecular engineering
- Process engineering

Civil engineering

- Environmental engineering
- Geotechnical engineering
- Structural engineering
- Transport engineering
- Water resources engineering

Electrical engineering

- Computer engineering
- Electronic engineering
- Optical engineering
- Power engineering

Mechanical engineering

- Acoustical engineering
- Manufacturing engineering
- Thermal engineering
- Vehicle engineering

Systems (interdisciplinary) engineering

- Aerospace engineering
- Agricultural engineering
- Applied engineering
- Biological engineering
- Building services engineering
- Energy engineering
- Railway engineering
- Industrial engineering
- Mechatronics
- Military engineering
- Nano engineering
- Nuclear engineering
- Petroleum engineering

Types of Articles submitted should be original research papers, not previously published, in one of the following categories,

- Applicational and design studies.
- Technology development,

– Comparative case studies.

– Reviews of special topics.

– Reviews of work in progress and facilities development.

– Survey articles.

– Guest editorials for special issues.

Ethic Responsibilities

The publication of an article in peer-reviewed *"International Journal of Engineering Technologies"* is an essential building block in the development of a coherent and respected network of knowledge. It is a direct reflection of the quality of the work. Peer-reviewed articles support and embody the scientific method. It is therefore important to agree upon standards of expected ethical behavior for all parties involved in the act of publishing: the author, the journal editor, the peer reviewer, the publisher and the society of society-owned or sponsored journals.

All authors are requested to disclose any actual or potential conflict of interest including any financial, personal or other relationships with other people or organizations within three years of beginning the submitted work that could inappropriately influence, or be perceived to influence, their work.

Submission of an article implies that the work described has not been published previously that it is not under consideration for publication elsewhere. The submission should be approved by all authors and tacitly or explicitly by the responsible authorities where the work was carried out, and that, if accepted, it will not be published elsewhere in the same form, in English or in any other language, including electronically without the written consent of the copyright-holder.

Upon acceptance of an article, authors will be asked to complete a "Copyright Form". Acceptance of the agreement will ensure the widest possible dissemination of information. An e-mail will be sent to the corresponding author confirming receipt of the manuscript together with a "Copyright Form" form or a link to the online version of this agreement.

Author Rights

As a journal author, you retain rights for a large number of author uses, including use by your employing institute or company. These rights are retained and permitted without the need to obtain specific permission from *IJET*. These include:

- ❖ The right to make copies (print or electronic) of the journal article for your own personal use, including for your own classroom teaching use;

- ❖ The right to make copies and distribute copies (including via e-mail) of the journal article to research colleagues, for personal use by such colleagues for scholarly purposes;

- ❖ The right to post a pre-print version of the journal article on internet web sites including electronic pre-print servers, and to retain indefinitely such version on such servers or sites for scholarly purposes

- ❖ the right to post a revised personal version of the text of the final journal article on your personal or institutional web site or server for scholarly purposes

- ❖ The right to use the journal article or any part thereof in a printed compilation of your works, such as collected writings or lecture notes.

Article Style

Authors must strictly follow the guide for authors, or their articles may be rejected without review. Editors reserve the right to adjust the style to certain standards of uniformity. Follow Title, Authors, Affiliations, Abstract, Keywords, Introduction, Materials and Methods, Theory/Calculation, Conclusions, Acknowledgements, References order when typing articles. The corresponding author should be identified with an asterisk and footnote. Collate

acknowledgements in a separate section at the end of the article and do not include them on the title page, as a footnote to the title or otherwise.

Abstract and Keywords:

Enter an abstract of up to 250 words for all articles. This is a concise summary of the whole paper, not just the conclusions, and is understandable without reference to the rest of the paper. It should contain no citation to other published work. Include up to six keywords that describe your paper for indexing purposes.

Abbreviations and Acronyms:

Define abbreviations and acronyms the first time they are used in the text, even if they have been defined in the abstract. Abbreviations such as IEEE, SI, MKS, CGS, sc, dc, and rms do not have to be defined. Do not use abbreviations in the title unless they are unavoidable.

Text Layout for Peer Review:

Use single column layout, double spacing and wide (3 cm) margins on white paper at the peer review stage. Ensure that each new paragraph is clearly indicated. Present tables and figure legends in the text where they are related and cited. Number all pages consecutively; use 12 pt font size and standard fonts; Times New Roman, Helvetica, or Courier is preferred.

Research Papers should not exceed 12 printed pages in two-column publishing format, including figures and tables.

Technical Notes and _Letters_ should not exceed 2,000 words.

Reviews should not exceed 20 printed pages in two-column publishing format, including figures and tables.

Equations:

Number equations consecutively with equation numbers in parentheses flush with the right margin, as in (1). To make equations more compact, you may use the solidus (/), the exp function, or appropriate exponents. Italicize Roman symbols for quantities and variables, but not Greek symbols. Use an dash (–) rather than a hyphen for a minus sign. Use parentheses to avoid ambiguities in denominators. Punctuate equations with commas or periods when they are part of a sentence, as in

$$C = a + b \tag{1}$$

Symbols in your equation should be defined before the equation appears or immediately following. Use "Eq. (1)" or "equation (1)," while citing.

Figures and Tables:

All illustrations must be supplied at the correct resolution:

* Black and white and colour photos - 300 dpi

* Graphs, drawings, etc - 800 dpi preferred; 600 dpi minimum

* Combinations of photos and drawings (black and white and color) - 500 dpi

In addition to using figures in the text, upload each figure as a separate file in either .tiff or .eps format during submission, with the figure number.

Table captions should be written in the same format as figure captions; for example, "Table 1. Appearance styles.". Tables should be referenced in the text unabbreviated as "Table 1."

References:

Please ensure that every reference cited in the text is also present in the reference list (and viceversa). Any references cited in the abstract must be given in full. Unpublished results and personal communications are not recommended in the reference list, but may be mentioned in the text. Citation of a reference as "in press" implies that the item has been accepted for publication. Number citations consecutively in square brackets [1]. Punctuation follows the bracket [2]. Refer simply to the reference number, as in [3]. Use "Ref. [3]" or Reference [3]" at the beginning of a sentence: "Reference [3] was …". Give all authors' names; use "et al." if there are six authors or more. For papers published in translated journals, first give the English citation, then the original foreign-language citation.

Books

[1]   J. Clerk Maxwell, *A Treatise on Electricity and Magnetism,* 3rd ed., vol. 2. Oxford:Clarendon Press, 1892, pp.68-73.

Journals

[2]   Y. Yorozu, M. Hirano, K. Oka, and Y. Tagawa, "Electron spectroscopy studies on magneto-optical media and plastic substrate interface", *IEEE Transl. J. Magn. Japan*, vol. 2, pp. 740-741, August 1987.

Conferences

[3]   Çolak I., Kabalci E., Bayindir R., and Sagiroglu S, "The design and analysis of a 5-level cascaded voltage source inverter with low THD", *2nd PowerEng Conference*, Lisbon, pp. 575-580, 18-20 March 2009.

Reports

[4]   IEEE Standard 519-1992, Recommended practices and requirements for harmonic control in electrical power systems, *The Institute of Electrical and Electronics Engineers*, 1993.

Text Layout for Accepted Papers:

A4 page margins should be margins: top = 24 mm, bottom = 24 mm, side = 15 mm. Main text should be given in two column. The column width is 87mm (3.425 in). The space between the two columns is 6 mm (0.236 in). Paragraph indentation is 3.5 mm (0.137 in). Follow the type sizes specified in Table. Position figures and tables at the tops and bottoms of columns. Avoid placing them in the middle of columns. Large figures and tables may span across both columns. Figure captions should be centred below the figures; table captions should be centred above. Avoid placing figures and tables before their first mention in the text. Use the abbreviation "Fig. 1," even at the beginning of a sentence.

Type size (pts.)	Appearance		
	Regular	**Bold**	*Italic*
10	Authors' affiliations, Section titles, references, tables, table names, first letters in table captions,figure captions, footnotes, text subscripts, and superscripts	**Abstract**	
12	Main text, equations, Authors' names, [a]		*Subheading (1.1.)*
24	Paper title		

Submission checklist:

It is hoped that this list will be useful during the final checking of an article prior to sending it to the journal's Editor for review. Please consult this Guide for Authors for further details of any item. Ensure that the following items are present:

❖ One Author designated as corresponding Author:

• E-mail address

• Full postal address

• Telephone and fax numbers

❖ All necessary files have been uploaded

• Keywords: a minimum of 4

• All figure captions (supplied in a separate document)

• All tables (including title, description, footnotes, supplied in a separate document)

❖ Further considerations

• Manuscript has been "spellchecked" and "grammar-checked"

• References are in the correct format for this journal

• All references mentioned in the Reference list are cited in the text, and vice versa

• Permission has been obtained for use of copyrighted material from other sources (including the Web)

• Color figures are clearly marked as being intended for color reproduction on the Web (free of charge) and in print or to be reproduced in color on the Web (free of charge) and in black-and-white in print.

Article Template Containing Author Guidelines for Peer-Review

First Author*, Second Author**‡, Third Author***

*Department of First Author, Faculty of First Author, Affiliation of First Author, Postal address

**Department of Second Author, Faculty of First Author, Affiliation of First Author, Postal address

***Department of Third Author, Faculty of First Author, Affiliation of First Author, Postal address

(First Author Mail Address, Second Author Mail Address, Third Author Mail Address)

‡ Corresponding Author; Second Author, Postal address, Tel: +90 312 123 4567, Fax: +90 312 123 4567,corresponding@affl.edu

Abstract- Enter an abstract of up to 250 words for all articles. This is a concise summary of the whole paper, not just the conclusions, and is understandable without reference to the rest of the paper. It should contain no citation to other published work. Include up to six keywords that describe your paper for indexing purposes. Define abbreviations and acronyms the first time they are used in the text, even if they have been defined in the abstract. Abbreviations such as IEEE, SI, MKS, CGS, sc, dc, and rms do not have to be defined. Do not use abbreviations in the title unless they are unavoidable.

Keywords- Keyword1; keyword2; keyword3; keyword4; keyword5.

2. Introduction

Authors should any word processing software that is capable to make corrections on misspelled words and grammar structure according to American or Native English. Authors may get help by from word

processor by making appeared the paragraph marks and other hidden formatting symbols. This sample article is prepared to assist authors preparing their articles to IJET.

Indent level of paragraphs should be 0.63 cm (0.24 in) in the text of article. Use single column layout, double-spacing and wide (3 cm) margins on white paper at the peer review stage. Ensure that each new paragraph is clearly indicated. Present tables and figure legends in the text where they are related and cited. Number all pages consecutively; use 12 pt font size and standard fonts; Times New Roman, Helvetica, or Courier is preferred. Indicate references by number(s) in square brackets in line with the text. The actual authors can be referred to, but the reference number(s) must always be given. Example: "..... as demonstrated [3, 6]. Barnaby and Jones [8] obtained a different result ...."

IJET accepts submissions in three styles that are defined as Research Papers, Technical Notes and Letter, and Review paper. The requirements of paper are as listed below:

➢ Research Papers should not exceed 12 printed pages in two-column publishing format, including figures and tables.

➢ Technical Notes and Letters should not exceed 2,000 words.

➢ Reviews should not exceed 20 printed pages in two-column publishing format, including figures and tables.

Authors are requested write equations using either any mathematical equation object inserted to word processor or using independent equation software. Symbols in your equation should be defined before the equation appears or immediately following. Use "Eq. (1)" or "equation (1)," while citing. Number equations consecutively with equation numbers in parentheses flush with the right margin, as in Eq. (1). To make equations more compact, you may use the solidus (/), the exp function, or appropriate exponents. Italicize Roman symbols for quantities and variables, but not Greek symbols. Use an dash (–) rather than a hyphen for a minus sign. Use parentheses to avoid ambiguities in denominators. Punctuate equations with commas or periods when they are part of a sentence, as in

$$C = a + b \tag{1}$$

Section titles should be written in bold style while sub section titles are italic.

3. Figures and Tables

3.1. *Figure Properties*

All illustrations must be supplied at the correct resolution:

➢ Black and white and colour photos - 300 dpi

➢ Graphs, drawings, etc - 800 dpi preferred; 600 dpi minimum

➢ Combinations of photos and drawings (black and white and colour) - 500 dpi

In addition to using figures in the text, Authors are requested to upload each figure as a separate file in either .tiff or .eps format during submission, with the figure number as Fig.1., Fig.2a and so on. Figures are cited as "Fig.1" in sentences or as "Figure 1" at the beginning of sentence and paragraphs. Explanations related to figures should be given before figure. Figures and tables should be located at the top or bottom side of paper as done in accepted article format.

Figure 1. Engineering technologies.

Table captions should be written in the same format as figure captions; for example, "Table 1. Appearance styles.". Tables should be referenced in the text unabbreviated as "Table 1."

Table 1. Appearance properties of accepted manuscripts

Type size (pts.)	Appearance		
	Regular	**Bold**	*Italic*
10	Authors' affiliations, Abstract, keywords, references, tables, table names, figure captions, footnotes, text subscripts, and superscripts	**Abstract**	
12	Main text, equations, Authors' names, Section titles		*Subheading (1.1.)*
24	Paper title		

4. Submission Process

The *International Journal of Engineering Technologies* operates an online submission and peer review system that allows authors to submit articles online and track their progress via a web interface. Articles that are prepared referring to this template should be controlled according to submission checklist given in "Guide f Authors". Editor handles submitted articles to IJET primarily in order to control in terms of compatibility to aims and scope of Journal.

Articles passed this control are checked for grammatical and template structures. If article passes this control too, then reviewers are assigned to article and Editor gives a reference number to paper. Authors registered to online submission system can track all these phases.

Editor also informs authors about processes of submitted article by e-mail. Each author may also apply to Editor via online submission system to review papers related to their study areas. Peer review is a critical element of publication, and one of the major cornerstones of the scientific process. Peer Review serves two key functions:

➢ Acts as a filter: Ensures research is properly verified before being published

➢ Improves the quality of the research

5. Conclusion

The conclusion section should emphasize the main contribution of the article to literature. Authors may also explain why the work is important, what are the novelties or possible applications and extensions. Do not replicate the abstract or sentences given in main text as the conclusion.

Acknowledgements

Authors may acknowledge to any person, institution or department that supported to any part of study.

References

[1] J. Clerk Maxwell, *A Treatise on Electricity and Magnetism*, 3rd ed., vol. 2. Oxford:Clarendon Press, 1892, pp.68-73. (Book)

[2] H. Poor, *An Introduction to Signal Detection and Estimation*, New York: Springer-Verlag, 1985, ch. 4. (Book Chapter)

[3] Y. Yorozu, M. Hirano, K. Oka, and Y. Tagawa, "Electron spectroscopy studies on magneto-optical media and plastic substrate interface", *IEEE Transl. J. Magn. Japan*, vol. 2, pp. 740-741, August 1987. (Article)

[4] E. Kabalcı, E. Irmak, I. Çolak, "Design of an AC-DC-AC converter for wind turbines", *International Journal of Energy Research*, Wiley Interscience, DOI: 10.1002/er.1770, Vol. 36, No. 2, pp. 169-175. (Article)

[5] I. Çolak, E. Kabalci, R. Bayindir R., and S. Sagiroglu, "The design and analysis of a 5-level cascaded voltage source inverter with low THD", *2nd PowerEng Conference*, Lisbon, pp. 575-580, 18-20 March 2009. (Conference Paper)

[6] IEEE Standard 519-1992, Recommended practices and requirements for harmonic control in electrical power systems, *The Institute of Electrical and Electronics Engineers*, 1993. (Standards and Reports)

Article Template Containing Author Guidelines for Accepted Papers

First Author*, Second Author**‡, Third Author***

*Department of First Author, Faculty of First Author, Affiliation of First Author, Postal address

**Department of Second Author, Faculty of First Author, Affiliation of First Author, Postal address

***Department of Third Author, Faculty of First Author, Affiliation of First Author, Postal address

(First Author Mail Address, Second Author Mail Address, Third Author Mail Address)

‡ Corresponding Author; Second Author, Postal address, Tel: +90 312 123 4567,

Fax: +90 312 123 4567,corresponding@affl.edu

Abstract- Enter an abstract of up to 250 words for all articles. This is a concise summary of the whole paper, not just the conclusions, and is understandable without reference to the rest of the paper. It should contain no citation to other published work. Include up to six keywords that describe your paper for indexing purposes. Define abbreviations and acronyms the first time they are used in the text, even if they have been defined in the abstract. Abbreviations such as IEEE, SI, MKS, CGS, sc, dc, and rms do not have to be defined. Do not use abbreviations in the title unless they are unavoidable.

Keywords Keyword1, keyword2, keyword3, keyword4, keyword5.

1. Introduction

Authors should any word processing software that is capable to make corrections on misspelled words and grammar structure according to American or Native English. Authors may get help by from word processor by making appeared the paragraph marks and other hidden formatting symbols. This sample article is prepared to assist authors preparing their articles to IJET.

Indent level of paragraphs should be 0.63 cm (0.24 in) in the text of article. Use single column layout, double-spacing and wide (3 cm) margins on white paper at the peer review stage. Ensure that each new paragraph is clearly indicated. Present tables and figure legends in the text where they are related and cited. Number all pages consecutively; use 12 pt font size and standard fonts; Times New Roman, Helvetica, or Courier is preferred. Indicate references by number(s) in square brackets in line with the text. The actual authors can be referred to, but the reference number(s) must always be given. Example: "..... as demonstrated [3,6]. Barnaby and Jones [8] obtained a different result ...."

IJET accepts submissions in three styles that are defined as Research Papers, Technical Notes and Letter, and Review paper. The requirements of paper are as listed below:

➢ Research Papers should not exceed 12 printed pages in two-column publishing format, including figures and tables.

➢ Technical Notes and Letters should not exceed 2,000 words.

➢ Reviews should not exceed 20 printed pages in two-column publishing format, including figures and tables.

Authors are requested write equations using either any mathematical equation object inserted to word processor or using independent equation software. Symbols in your equation should be defined before the equation appears or immediately following. Use "Eq. (1)" or "equation (1)," while citing. Number equations consecutively with equation numbers in parentheses flush with the right margin, as in Eq. (1). To make equations more compact, you may use the solidus (/), the exp function, or appropriate exponents. Italicize Roman symbols for quantities and variables, but not Greek symbols. Use an dash (-) rather than a hyphen for a

minus sign. Use parentheses to avoid ambiguities in denominators. Punctuate equations with commas or periods when they are part of a sentence, as in

$$C = a + b \qquad (1)$$

Section titles should be written in bold style while sub section titles are italic.

6. Figures and Tables

6.1. Figure Properties

All illustrations must be supplied at the correct resolution:

➢ Black and white and colour photos - 300 dpi

➢ Graphs, drawings, etc - 800 dpi preferred; 600 dpi minimum

➢ Combinations of photos and drawings (black and white and colour) - 500 dpi

In addition to using figures in the text, Authors are requested to upload each figure as a separate file in either .tiff or .eps format during submission, with the figure number as Fig.1., Fig.2a and so on. Figures are cited as "Fig.1" in

sentences or as "Figure 1" at the beginning of sentence and paragraphs. Explanations related to figures should be given before figure.

Fig. 1. Engineering technologies.

Figures and tables should be located at the top or bottom side of paper as done in accepted article format. Table captions should be written in the same format as figure captions; for example, "Table 1. Appearance styles.". Tables should be referenced in the text unabbreviated as "Table 1."

Table 1. Appearance properties of accepted manuscripts

Type size (pts.)	Appearance		
	Regular	**Bold**	*Italic*
10	Main text, section titles, authors' affiliations, abstract, keywords, references, tables, table names, figure captions, equations, footnotes, text subscripts, and superscripts	**Abstract-**	*Subheading (1.1.)*
12	Authors' names,		
24	Paper title		

6.2. Text Layout for Accepted Papers

A4 page margins should be margins: top = 24 mm, bottom = 24 mm, side = 15 mm. The column width is 87mm (3.425 in). The space between the two columns is 6 mm (0.236 in). Paragraph indentation is 3.5 mm (0.137 in). Follow the type sizes specified in Table. Position figures and tables at the tops and bottoms of columns. Avoid placing them in the middle of columns. Large figures and tables may span across both columns. Figure captions should be centred below the figures; table captions should be centred above. Avoid placing figures and tables before their first mention in the text. Use the abbreviation "Fig. 1," even at the beginning of a sentence.

7. Submission Process

The International Journal of Engineering Technologies operates an online submission and peer review system that allows authors to submit articles online and track their progress via a web interface. Articles that are prepared referring to this template should be controlled according to submission checklist given in "Guide f Authors". Editor handles submitted articles to IJET primarily in order to control in terms of compatibility to aims and scope of Journal. Articles passed this control are checked for grammatical and template structures. If article passes this control too, then reviewers are assigned to article and Editor gives a reference number to paper. Authors registered to online submission system can track all these phases. Editor also informs authors about processes of submitted article by e-mail. Each author may also apply to Editor via online

submission system to review papers related to their study areas. Peer review is a critical element of publication, and one of the major cornerstones of the scientific process. Peer Review serves two key functions:

➢ Acts as a filter: Ensures research is properly verified before being published

➢ Improves the quality of the research

8. Conclusion

The conclusion section should emphasize the main contribution of the article to literature. Authors may also explain why the work is important, what are the novelties or possible applications and extensions. Do not replicate the abstract or sentences given in main text as the conclusion.

Acknowledgements

References

[7] J. Clerk Maxwell, A Treatise on Electricity and Magnetism, 3rd ed., vol. 2. Oxford:Clarendon Press, 1892, pp.68-73. (Book)

[8] H. Poor, An Introduction to Signal Detection and Estimation, New York: Springer-Verlag, 1985, ch. 4. (Book Chapter)

[9] Y. Yorozu, M. Hirano, K. Oka, and Y. Tagawa, "Electron spectroscopy studies on magneto-optical media and plastic substrate interface", IEEE Transl. J. Magn. Japan, vol. 2, pp. 740-741, August 1987. (Article)

[10] E. Kabalcı, E. Irmak, I. Çolak, "Design of an AC-DC-AC converter for wind turbines", International Journal of Energy Research, Wiley Interscience, DOI: 10.1002/er.1770, Vol. 36, No. 2, pp. 169-175. (Article)

[11] I. Çolak, E. Kabalci, R. Bayindir R., and S. Sagiroglu, "The design and analysis of a 5-level cascaded voltage source inverter with low THD", 2nd PowerEng Conference, Lisbon, pp. 575-580, 18-20 March 2009. (Conference Paper)

[12] IEEE Standard 519-1992, Recommended practices and requirements for harmonic control in electrical power systems, The Institute of Electrical and Electronics Engineers, 1993. (Standards and Reports)

INTERNATIONAL JOURNAL OF ENGINEERING TECHNOLOGIES (IJET)
COPYRIGHT AND CONSENT FORM

This form is used for article accepted to be published by the IJET. Please read the form carefully and keep a copy for your files.

TITLE OF ARTICLE (hereinafter, "The Article"):

………..……………………………………….............…………………………………………………

………..……………………………………….............……………………………………………………

………..…………………………………………………….…………………………………………………

LIST OF AUTHORS:

………..…………………………………………………..…………………………………………………

………..…………………………………….............…………………………………………………………

………..…………………………………………………………………………………….………………

CORRESPONDING AUTHOR'S ("The Author") NAME, ADDRESS, INSTITUTE AND EMAIL:

………..……………………………………………….…………………………………………………

………..………………………………………….............……………………………………………………

………..………………………………………………….…………………………………….……

COPYRIGHT TRANSFER

The undersigned hereby transfers the copyright of the submitted article to International Journal of Engineering Technologies (the "IJET"). The Author declares that the contribution and work is original, and he/she is authorized by all authors and/or grant-funding agency to sign the copyright form. Author hereby assigns all including but not limited to the rights to publish, distribute, reprints, translates, electronic and published derivates in various arrangements or any other versions in full or abridged forms to IJET. IJET holds the copyright of Article in its own name.

Author(s) retain all rights to use author copy in his/her educational activities, own websites, institutional and/or funder's web sites by providing full citation to final version published in IJET. The full citation is provided including Authors list, title of the article, volume and issue number, and page number or using a link to the article in IJET web site. Author(s) have the right to transmit, print and share the first submitted copies with colleagues. Author(s) can use the final published article for his/her own professional positions, career or qualifications by citing to the IJET publication.

Once the copyright form is signed, any changes about the author names or order of the authors listed above are not accepted by IJET.

   Authorized/Corresponding Author   **Date/ Signature**